




Article

Studies of Various Batch Adsorption Parameters for the Removal of Trypan Blue Using Ni-Zn-Bi-Layered Triple Hydroxide and Their Isotherm, Kinetics, and Removal Mechanism

Ganesan Sriram ^{1,*}, Nimisha Baby ¹, Karmegam Dhanabalan ¹, Muthuraj Arunpandian ¹, Karuppaiah Selvakumar ², Thangarasu Sadhasivam ¹ and Tae Hwan Oh ^{1,*}

¹ School of Chemical Engineering, Yeungnam University, Gyeongsan 38541, Republic of Korea

² Department of Physiology, Saveetha Dental College and Hospitals, Saveetha Institute of Medical and Technical Science (SIMATS), Saveetha University, Chennai 600077, India

* Correspondence: sriramyu@yu.ac.kr (G.S.); taehwanoh@ynu.ac.kr (T.H.O.)

Abstract: The present study addressed the removal of Trypan blue (TB) from water using a novel Ni-Zn-Bi-layered triple hydroxide (NZB LTH or NZB) synthesized through the co-precipitation technique. The physiochemical properties of NZB were analyzed before and after TB adsorption using XRD, BET, FESEM, FTIR-ATR, Raman, and XPS. Studies on adsorption indicate that 80 mg of NZB has a maximum TB removal effectiveness of around 96.7% at natural pH (~4.5–5.0). This study found that NZB has a maximum adsorption capacity (q_{\max}) of $5.3 \text{ mg}\cdot\text{g}^{-1}$ at dye concentrations ranging from 5 to $30 \text{ mg}\cdot\text{L}^{-1}$. When combined with various anionic dye mixtures, NZB's selectivity studies showed that it is highly selective for the removal of TB and is also effective at removing cationic dyes. When compared to Na_2SO_4 and NaCl salts, NZB had a lower dye removal percentage for TB removal in the presence of Na_2SO_3 . In an adsorption process, the interaction between the TB and NZB in an aqueous solution is caused by hydrogen bonding and electrostatic interactions, which are investigated in the adsorption mechanism. In comparison with ethanol and methanol, the recyclability investigation of NZB revealed the notable removal of TB using 0.1 M NaOH for the desorption. Therefore, the present investigation suggests that NZB is an appropriate adsorbent for the removal of TB from an aqueous solution.

Keywords: synthesis; co-precipitation; dye removal; anionic dye; LTH; adsorption capacity; selectivity; salt-effect; reusability



Citation: Sriram, G.; Baby, N.; Dhanabalan, K.; Arunpandian, M.; Selvakumar, K.; Sadhasivam, T.; Oh, T.H. Studies of Various Batch Adsorption Parameters for the Removal of Trypan Blue Using Ni-Zn-Bi-Layered Triple Hydroxide and Their Isotherm, Kinetics, and Removal Mechanism. *Inorganics* **2024**, *12*, 296. <https://doi.org/10.3390/inorganics12110296>

Academic Editor: Eleonora Aneggi

Received: 14 October 2024

Revised: 9 November 2024

Accepted: 15 November 2024

Published: 19 November 2024



Copyright: © 2024 by the authors. Licensee MDPI, Basel, Switzerland. This article is an open access article distributed under the terms and conditions of the Creative Commons Attribution (CC BY) license (<https://creativecommons.org/licenses/by/4.0/>).

1. Introduction

Dye contamination of water necessitates treatment by removing the dyes with diverse adsorbents or methods before they discharge into local drainage systems or natural water bodies [1–3]. Various industries, such as textiles, cosmetics, ink, plastics, paper, food, pharmaceuticals, pulp, leather, printing, paints, and rubber, use dyes because they are easily soluble in water and give concentrated color to the water [4,5]. Trypan blue (TB) is a water-soluble azo dye that is used for biological staining, vitreoretinal surgery, and measuring cell viability, and it is also used in the food coloring dyeing process [6–8]. However, TB is toxic to cells for a short period of exposure time and carcinogenic to humans and animals; if exhaled or ingested, it causes eye agitation, skin irritation, and digestive problems. Excessive levels of TB may harm aquatic life. Due to the toxic effects of TB, the European Chemicals Agency has determined that TB is carcinogenic to human beings and requested that its usage in testing facilities be restricted [9]. Discharging untreated water polluted with this dye may have detrimental effects on natural water resources, disrupt the aquatic lifecycle, and pose substantial risks to human health, including toxicological and carcinogenic effects. To prevent contamination of the environment, the TB discharges from various sectors should be removed from the water. This concern of dye contaminations in water has led

to the development of many water treatments, such as advanced oxidation processes, ion exchange, deep eutectic solvent, coagulation-flocculation, adsorption, electrocoagulation, wet-oxidation, sedimentation, arc discharge, membrane bioreactors, phytoremediation, reverse osmosis, sequencing batch reactors, membrane filtration, etc. [8,10–17]. Among these, adsorption is considered to be one of the easiest, low-cost, most rapid, and effective approaches to removing dyes from water using adsorbents [18–20].

The process of adsorption is capable of efficiently removing many kinds of pollutants [21–25]. In addition, the application of this technique in the removal of dyes from water-based solutions may be seen visibly in an instant. Adsorbents with a substantial surface area, extensive porous architectures, and abundant surface hydroxyl groups have the potential to expeditiously remove dyes. Consequently, an extensive study has been conducted to develop adsorbents for the goal of removing harmful dyes and other pollutants. These adsorbents include porous carbon derived from biomass, activated carbon from bamboo fibers, carbon xerogel, silica xerogel, agricultural wastes, hydrogels, metal-organic frameworks (MOFs), biochar, calcium silicate, aerogel, zeolite, polymers, natural adsorbents, layered double hydroxides (LDHs), montmorillonite, layered triple hydroxides (LTHs), red mud waste, nanoparticles, and various other adsorbents [12,18,26–41]. Among these adsorbents, LTHs possess a high positive charge, nanosheet configuration, high porosity, abundant surface functional groups, and a moderate surface area. Additionally, they are synthesized using low-cost chemicals and inexpensive methods, making them a promising and cost-effective option for effectively removing anionic-based dyes. The advantages of LTHs means they can be used to effectively treat water contaminated with anionic-based dyes.

Recently, nanomaterials have been explored for environmental applications because of their distinctive features, primarily their high surface-to-volume ratio. Accordingly, because of their layered structure and three cationic constituents, LTHs are one of the nanomaterials that are becoming more popular among researchers working with water research [42–44]. Conversely, LDHs, which are a mixture of two cationic precursors, would be less efficient than LTHs due to the possibility of reduced surface area and low functional groups [45–48]. As a result, three cationic structures with LTHs could be able to remove dye more effectively than LDHs. Due to their unique characteristics, the applications for LTHs include water purification, supercapacitors, batteries, electrolysis, photocatalysts, electrocatalysts, and water splitting [49–61]. The LTH structure has notable qualities, such as a large number of active sites and high interlayer space, as well as a remarkable ability for efficient ion exchange. Thus, water research communities are focusing on these LTHs to use them as active adsorbents for water purification.

It has been reported in several studies that LTHs are used for the removal of dyes. Accordingly, Kazemi et al. synthesized a MgZnAl LTH using the hydrothermal method to remove acid yellow 76 (AY76) at pH 4 [38]. Because of the electrostatic interaction and hydrogen bonding between the LTHs and AY76, the maximum adsorption capacity (q_{\max}) of the LTHs was found to be $277.8 \text{ mg}\cdot\text{g}^{-1}$, and they had a high reusability of 90.3% after four cycles. Recently, Abdel-Hady et al. produced ZnMgAl LTHs via co-precipitation to remove crystal violet (CV) at a pH of 9 [62]. However, the q_{\max} of the prepared LTHs adsorbent was only $64.8 \text{ mg}\cdot\text{g}^{-1}$, which was a result of its ineffectiveness at removing the positively charged CV dye. In contrast, after five cycles, the reusability of ZnMgAl LTHs was determined to be moderate at 64.0%. However, the potential mechanisms that facilitated adsorption between ZnMgAl LTHs and CV exhibited substantial efficacy, such as mesoporous filling, surface diffusion, hydrogen bonding, electrostatic interaction, and π - π interaction. Using the co-precipitation method, Bahadi et al. synthesized a polyethyleneimine-functionalized graphene oxide composite with MgFeAl LTHs (PEI@GO/MgFeAl) to remove acid red 1 (AR1) dye at pH 6 [43]. AR1 adsorbed on PEI@GO/MgFeAl exhibited a q_{\max} of $225.7 \text{ mg}\cdot\text{g}^{-1}$, and an effective reusability of 80.7% was observed after five cycles. The adsorption of AR1 was achieved by the mechanism of electrostatic interactions, pore-filling, hydrogen bonding, and π - π interactions. Similarly, co-

precipitation was employed to synthesize MgNiAl-CO₃, which was then calcined at 500 °C to yield MgNiAl-C to remove methyl orange (MO) at pH 8 [63]. Because of the calcination effect, MgNiAl-C (375.4 mg·g⁻¹) had a higher q_{\max} than MgNiAl-CO₃ (118.5 mg·g⁻¹) for MO removal. Similarly, co-precipitation was used to produce NiMgAl LTHs with variable percentages (20% and 30%) of Ni(NO₃)₂·6H₂O, which were then calcined at 400 °C to obtain NiMgAl-layered triple oxides (LTOs) to remove MO at pH 9 [64]. This work demonstrated increased Ni(NO₃)₂·6H₂O loading into MgAl, as well as improved adsorption performance following calcination. After calcination, 30%NiMgAl LTO (322.5 mg·g⁻¹) had a higher q_{\max} compared to 20%NiMgAl LTO (270.2 mg·g⁻¹), 20%NiMgAl LTHs (250.0 mg·g⁻¹), and 30%NiMgAl LTHs (232.5 mg·g⁻¹). In contrast to the 30%NiMgAl LTHs, which only removed 58% of the MO after three cycles, the 30%NiMgAl LTO was able to remove 72% of the MO. On the other hand, samples of LTHs still showed a good q_{\max} , and they offer the following advantages over LTO: a low-temperature process, no calcination or annealing is necessary, a time-saving procedure, high hydroxyl groups on their surface that are crucial for the removal of dyes through hydrogen bonding and electrostatic interaction, mild-temperature drying following synthesis does not impact structure or morphology, the ability to synthesize LTHs using a single method, and a high crystalline structure. For this reason, the use of LTH-based adsorbents for dye removal via the adsorption process has the potential to achieve a high adsorption capacity for dye removal. According to the above studies, LTHs are often synthesized via co-precipitation, which is a low-cost approach, and this type of method is advantageous for the adsorption process since it produces inexpensive and efficient sorbents. The pH of the solution is crucial for the adsorption process and should not harm the environment. Using a pH of the dye solution between 4 and 8 for the adsorption process would be environmentally friendly. However, some studies performed at pH 9 could be harmful. Further, it is necessary to test the reusability of the adsorbent in the adsorption process, which helps to reduce the material waste or cost of the process. Therefore, it is necessary to desorb the dye molecules from the adsorbent surface by either chemical or thermal methods. It would be preferable if the adsorbent could be reused for at least five cycles, ensuring a high removal efficiency of over 90%. Additionally, the q_{\max} is dependent on the volume and dosage of the adsorbents, as well as on the concentration of the dye molecules. For the higher q_{\max} , experiments could use a high volume of dye solution, a low adsorbent dosage, and a higher dye concentration.

This is the first time NZB has been synthesized using co-precipitation to remove TB from an aqueous solution. Several characterization approaches were employed to compare before and after dye adsorption. To investigate the dye removal effectiveness and potential mechanisms of the synthesized adsorbent, a systematic batch adsorption procedure was carried out, accounting for the effects of pH, dosage, dye concentrations, time, isotherms, and kinetic studies. Additionally, the study involves the process of selectively removing TB by combining various dye mixtures, the salt effect, and exploring the potential for reusing the materials. The potential of NZB as an effective adsorbent in the treatment of aqueous solutions contaminated with both anionic and cationic dyes is demonstrated by this study. Figure 1 presents a diagram of the synthesis of NZB and its ensuing removal of TB.

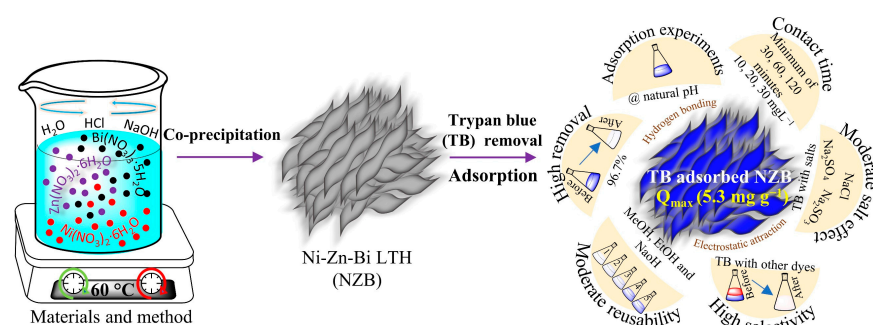


Figure 1. Schematic diagram of the synthesis of NZB and its adsorption properties regarding TB.

2. Results and Discussion

The adsorbent's surface area could potentially assist in achieving a faster and higher level of dye removal. Thus, an analysis was conducted on the surface area of the NZB using the N_2 adsorption–desorption technique and the Barrett–Joyner–Halenda (BJH) method to assess the porosity of the adsorbent before TB adsorption. As shown in Figure 2a, according to the IUPAC classification, the NZB shows a Type IV isotherm curve with a characteristic H3 hysteresis loop opening at 0.45 (P/P_0) and closing at 1.0 (P/P_0), demonstrating the presence of a mesoporous structure on the surfaces. This loop represents the capillary condensation properties occurring in the mesopores. The NZB's surface area was determined to be low, at $17.08 \text{ m}^2 \cdot \text{g}^{-1}$, whereas the pore volume and pore diameter were found to be $0.0436 \text{ cm}^3 \cdot \text{g}^{-1}$ and 5.9 nm , respectively. The lower surface area might be owing to the presence of moisture, which can block the pores and reduce surface area. However, the layered triple hydroxide (LTH) type of materials may have high positive charges on their external surfaces, and this could play a crucial role in the removal of a large number of anionic dye molecules rather than their surface area. A similar result was obtained in the report of the N_2 adsorption–desorption isotherm study on the HKUST-1 and HHK-10 before and after water vapor adsorption. The surface area of these MOF materials was 1510 and $1284 \text{ m}^2 \cdot \text{g}^{-1}$, respectively. After water vapor adsorption, the surface area decreased to 607 and $687 \text{ m}^2 \cdot \text{g}^{-1}$. As a result, the presence of moisture could reduce the material's surface area [65]. In light of this, NZB has the potential to function as an effective adsorbent in the process of water treatment for the removal of TB.

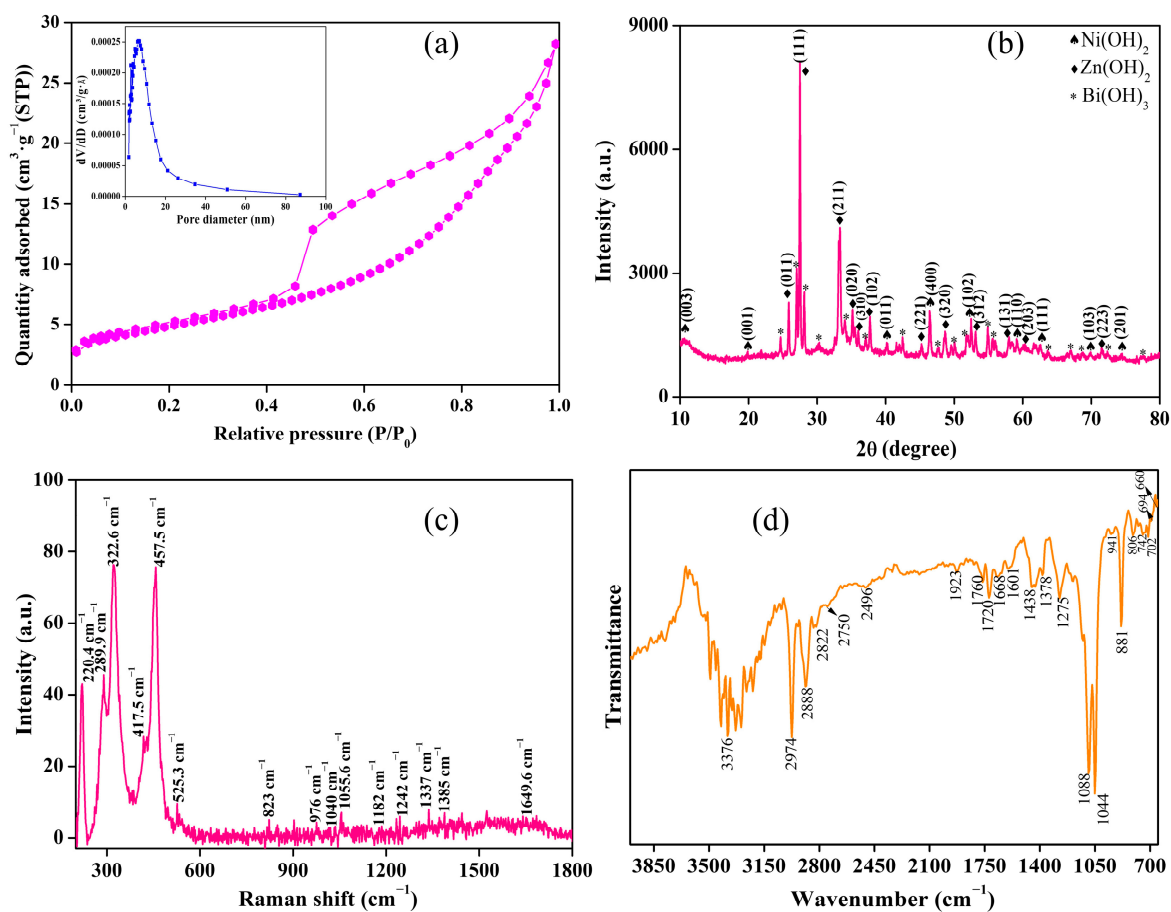


Figure 2. Characterization of NZB LTH before dye adsorption: (a) the nitrogen (N_2) adsorption–desorption isotherm curve and porosity measurement by Barrett–Joyner–Halenda (BJH) plot (inset); (b) XRD pattern; (c) Raman spectrum; and (d) FTIR-ATR spectrum.

X-ray diffraction (XRD) is a non-destructive method for material structural investigation. Figure 2b presents the XRD analysis of the structural matter of NZB before TB adsorption. The XRD pattern of NZB revealed a crystalline structure. Accordingly, Ni(OH)₂ was confirmed by the presence of characteristic peaks at 2 θ , including 11.7°, 19.2°, and 38.2° and 46.4°, 52.4°, 59.2°, 62.5°, 69.8°, and 74.3°, denoted as (003), (001), and (011) and (400), (102), (110), (111), (103), and (201), respectively [3,66–68]. The appearance of peaks like (011), (111), (211), (020), (310), (102), (221), (320), (312), (131), (203), and (223) confirms Zn(OH)₂, which corresponds to 25.8°, 27.3°, 33.3°, 35.2°, 36.0°, 37.6°, 45.1°, 48.7°, 53.0°, 57.9°, 60.3°, and 71.4°, respectively [69–71]. Furthermore, the earlier reports confirmed that all remaining characteristic peaks were indeed Bi(OH)₃ [72–74]. However, some noise in the diffraction pattern can be seen due to the presence of moisture on the NZB. The presence of characteristic peaks of respective hydroxides such as Ni(OH)₂, Zn(OH)₂, and Bi(OH)₃ in the diffraction pattern confirms the LTH structure in NZB. Furthermore, Raman spectroscopy was utilized to examine and govern the NZB's functional composition. Figure 2c shows the Raman spectrum of the adsorbent, NZB, which covers from 200 to 1800 cm⁻¹. The Raman shift at 220.4 cm⁻¹ for Bi-OH, 289.9 and 322.6 cm⁻¹ for Zn-OH, and 417.5, 457.7, and 525.3 cm⁻¹ for Ni-OH showed the existence of M-OH (Metal-hydroxide) stretching vibration in the adsorbent [70,75,76]. The peaks at 976, 823, 1040, 1337–1385, and 1649 cm⁻¹ are ascribed to NO₃⁻ in-plane bending, symmetric stretching, antisymmetric stretching, and out-of-plane bending vibration, respectively [77,78]. Additional peaks at 1055.6 cm⁻¹ and 1182 cm⁻¹ to 1242 cm⁻¹ were due to the symmetric and antisymmetric vibration of carbonate ions (CO₃²⁻) [78]. The observation of these peaks verifies the LTHs' composition of Ni(OH)₂, Zn(OH)₂, and Bi(OH)₃ in their structure.

The functional groups in NZB were found using FTIR-ATR. Figure 2d thus reveals the IR peaks of NZB in the wavenumber range of 650 to 4000 cm⁻¹. The wider peak at 3200–3500 cm⁻¹ was produced by stretching vibrations of interlayer hydroxyl (-OH) groups from the NZB. The peaks at 2974, 2750, 2496, 1923, 1088, and 1438 cm⁻¹ indicate strong and mild C-H stretching vibrations, while the peak from 2822 to 2882 cm⁻¹ represents CH₂ stretching [3,79]. The characteristic peaks at 1378 and 1275 cm⁻¹ correspond to the symmetric stretching vibrations of NO₃⁻ ion and 1044 cm⁻¹ to the symmetric stretching vibration of CO₃²⁻ ion, respectively [3,79–81]. The symmetric stretching vibration of the carboxylate molecule results in an IR peak regarding 1720–1767 cm⁻¹ [82]. The peak between 1601 and 1668 cm⁻¹ is caused by the bending vibration of water molecules [83]. The peaks at 941 and 881 cm⁻¹ correspond to the metal-oxygen and metal-hydroxyl groups in LTHs [84]. The absorption peaks in the 806–660 cm⁻¹ range may be related to the vibrational modes of O-M-O and M-O-M, where M denotes Ni, Zn, and Bi [80]. The presence of the peaks mentioned above served as evidence that several functional groups are present in NZB LTHs.

Furthermore, this study analyzed the NZB's morphology and elemental composition using FESEM and EDX. Accordingly, Figure 3a–c shows the morphology of the NZB at various scale ranges, such as 5 μ m, 1 μ m, and 500 nm. The observed layered structure and predicted flat sheet-type morphologies were noted. The rough surface was produced and the stacked sheet layer of NZB was identified at 500 nm scale. However, particles or grains were seen on the NZB's surface. This could be because the particles were crushed into a fine powder after the material was made. The sizes of these particles or grains could be between 100 and 500 nm. These sheet structures could have more active sites and surface areas, which might be beneficial for removing a considerable amount of dye molecules from water. The elemental mapping result shows that the NZB's distribution of Ni, Zn, Bi, and O is uniform (Figure 3d–g). These mapping pictures show that NZB has a higher concentration of Ni than Zn, Bi, and O elements, which is confirmed by the quantity of each chemical used in the preparation. Figure 3h depicts the NZB's elemental composition. The EDX spectrum revealed that the weight percentage of Ni K (53.78%) was larger than Zn K (29.46%), Bi M (6.35%), and O K (10.4%), and no further elements were identified,

suggesting that NZB is produced only from the nickel-zinc-bismuth composition. Similarly, the proportion of NZB's atomic weight % was identified as Ni K > Zn K > O K > Bi M.

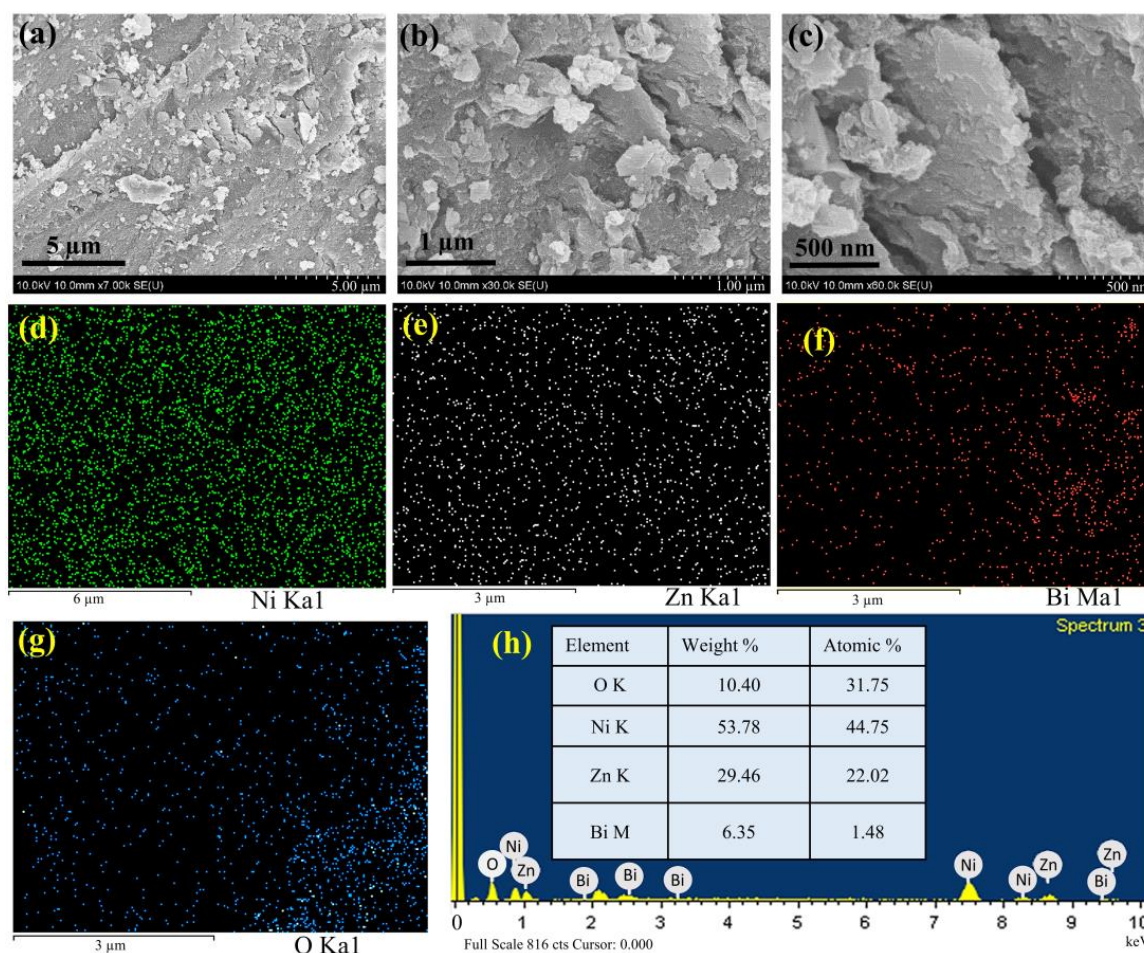


Figure 3. Characterization of NZB before dye adsorption: (a–c) FESEM images at different scales of 5 μm , 1 μm , and 500 nm; (d–g) elemental mapping; and (h) EDX spectrum with the table of element weights and atomic percentages.

XPS was used to determine the existence of the elemental composition on the produced adsorbent. The Ni-Zn-Bi LTH (NZB) of the full XPS survey spectrum is depicted in Figure 4a. The spectrum was analyzed within the binding energy range of 0 to 1200 eV, and the presence of NZB elements, including Bi 4f, C 1s, O 1s, Ni 2p, and Zn 2p, was confirmed at specific binding energies. Moreover, Figure 4b–f demonstrated the high resolution of each NZB component present at corresponding binding energies; the discussion of these peaks follows. The high-resolution spectrum of Bi 4f confirms two distinctive peaks at 157.7 eV and 163.1 eV, which are caused by Bi 4f_{7/2} and Bi 4f_{5/2}, respectively. In the C1s peaks of the high-resolution spectrum, two peaks were observed at 284.2 eV and 288.3 eV. This was a result of the carbon bonding of the HCO₃[−] and CO₃^{2−} within the interlayer of NZB LTHs [85]. In contrast, O 1s exhibits a single characteristic peak at 530.5 eV, which is attributed to the M-OH (M=Ni-Zn-Bi) bonding. Consequently, the presence of this peak demonstrates that the hydroxyl group of water is bonded to the surface of the NZB LTHs. The Ni 2p spectrum exhibits the two peaks of Ni 2p_{3/2} and Ni 2p_{1/2} at binding energies of 855.0 eV and 872.7 eV, respectively. Furthermore, the Ni 2p is accompanied by the formation of satellite peaks at 860.6 eV and 878.9 eV. Lastly, the binding energies of Zn 2p_{3/2} and Zn 2p_{1/2}, respectively, assigned two peaks to the Zn 2p spectrum at 1020.9 eV

and 1044.0 eV, indicating the presence of Zn²⁺ in NZB LTHs. Therefore, the presence of the aforementioned elements confirmed the synthesized Ni-Zn-Bi-layered triple hydroxide.

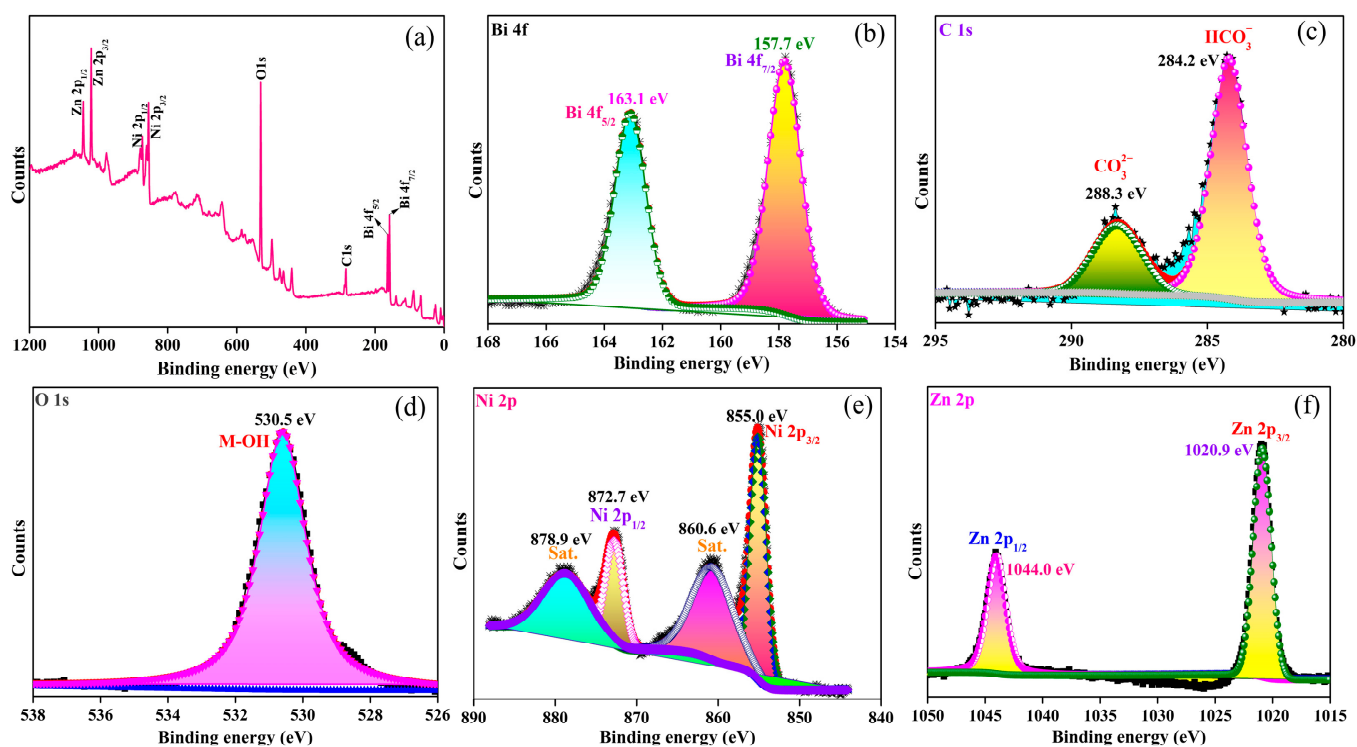


Figure 4. NZB LTH XPS spectra before dye adsorption: (a) Full survey spectrum and high-resolution spectrum of (b) Bi 4f, (c) C 1s, (d) O 1s, (e) Ni 2p, and (f) Zn 2p.

3. Batch Adsorption

3.1. pH

The adsorption process for the removal of dye from water may be influenced by the pH of the solution. Thus, it is crucial to investigate TB adsorption at various pH levels. Figure 5a shows the percentage of dye removed at various pH levels using 80 mg of NZB and 15 mg·L⁻¹ of TB concentration. The dye removal percentage dropped steadily from 97.6% to 12.3% as the pH increased from 2 to 10. The higher removal (97.6%) at pH 2 was due to the higher protonation ($-\text{OH}^{2+}$) of NZB surfaces that may be highly attracted with TB molecules through hydrogen bonding with chemical structures such as $-\text{OH}$, $-\text{NH}_2$, and $-\text{N}=\text{N}-$ and also capable of high interaction with negatively charged sulfonate ($-\text{SO}_3^-$) groups (Figure S1). The decrease in removal efficiency from 96.2% to 12.3% from pH 4 to 10 may be attributed to the increasing deprotonation ($-\text{OH}^{2-}$) on NZB surfaces, which are unable to attract negatively charged groups in dye structures. Figure S2 represents the UV-Vis absorbance spectra of TB at various pHs, as well as spectra before and after TB adsorption by NZB, showing that the absorbance peak was substantially reduced in acidic conditions (2, 4, and natural pH (~4.5–5.0)), indicating strong adsorption. In contrast, the spectra obtained in the base media exhibit increased absorption peaks, indicating restricted adsorption. NZB surfaces may contain vast positive charges ($-\text{OH}^+$) in acidic environments, electrostatically attracting or hydrogen bonding with the TB dye. However, when the pH increases (natural (~4.5–5.0) and 6–10), they acquire negative charges ($-\text{OH}^-$), repelling the TB. Furthermore, at natural pH, the dye removal percentage was found to be 87.9%, which is significant. As a result, accomplishing an adsorption procedure in either an acidic or basic medium may affect the environment; hence, subsequent adsorption experiments were undertaken using natural pH (~4.5–5.0).

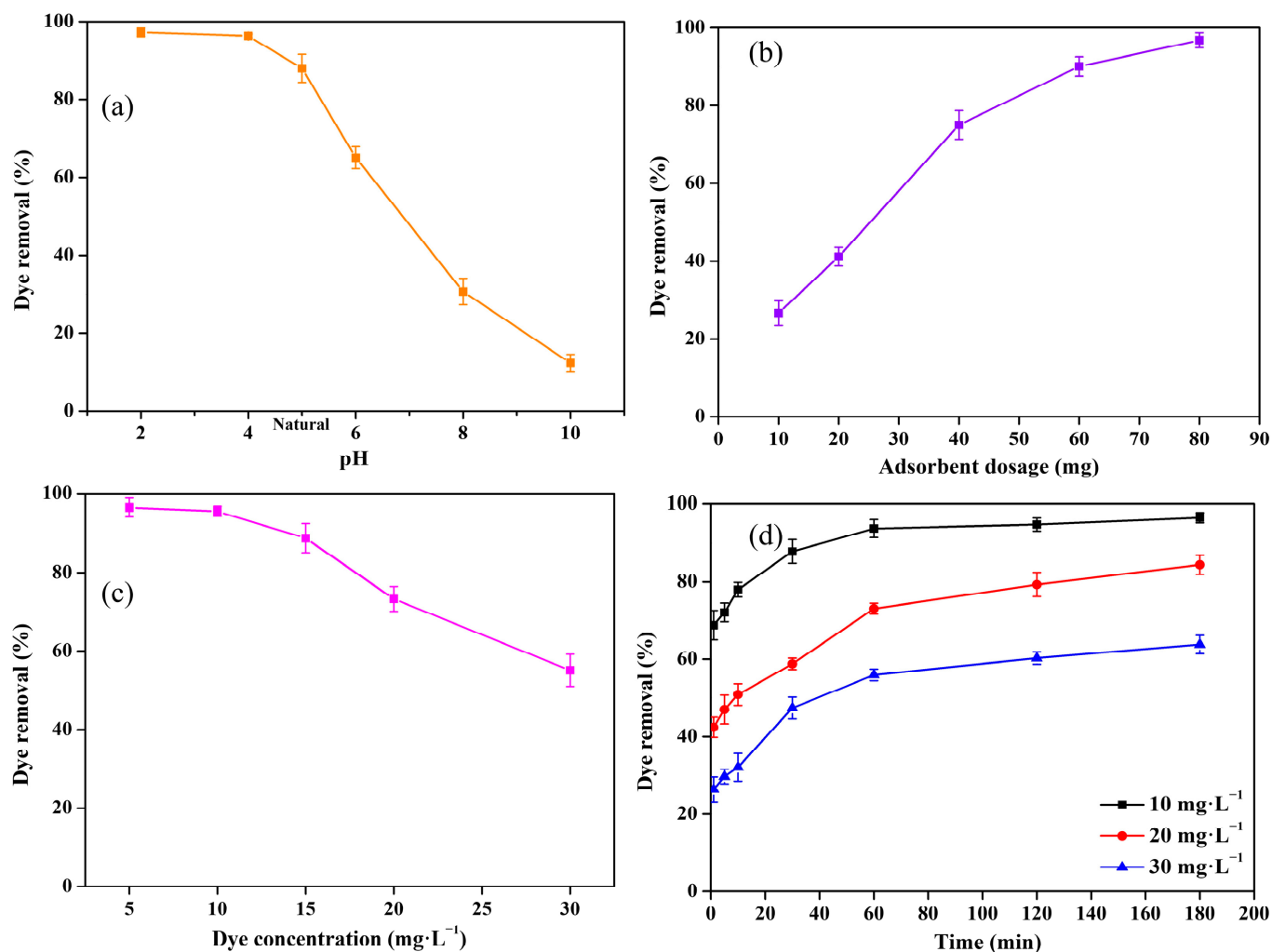


Figure 5. Batch adsorption parameters for dye (TB) removal using NZB LTH at room temperature: (a) effect of pH (Dosage: 80 mg, dye concentration: 15 mg·L⁻¹, volume: 25 mL, time: 1 h); (b) effect of adsorbent dosage (Dye concentration: 10 mg·L⁻¹, pH: natural (~4.5–5.0), volume: 25 mL, time: 1 h); (c) effect of dye concentration (Dosage: 80 mg, pH: natural (~4.5–5.0), volume: 25 mL, time: 1 h); and (d) effect of contact time (Dosage: 80 mg, pH: natural (~4.5–5.0), volume: 25 mL, dye concentration: 10, 20 and 30 mg·L⁻¹) at different dye concentrations.

3.2. Adsorbent Dosage

The adsorbent dosage may be important in the adsorption process for dye removal. Therefore, an experiment was performed to test the influence of NZB dosage on dye removal. The dosage ranged from 10 to 80 mg, with a dye concentration of 10 mg·L⁻¹ at natural solution pH (~4.5–5.0). Figure 5b shows the dye removal percentage plotted against the adsorbent dosage. As the NZB's dosage increased from 10 to 80 mg, the dye removal percentage increased steadily from 26.6% to 96.7%. The results show that increasing the adsorbent dosage resulted in a considerable increase in adsorbent sites, which was attributed to a higher dye removal percentage. Figure S3 depicts absorbance spectra both before and after TB adsorption by NZB at various dosages; the UV-Vis absorbance peak significantly decreased when the NZB dosage increased from 10 to 80 mg. The ideal dosage of 80 mg was determined via these studies and utilized in subsequent investigations.

3.3. Dye Concentration

The increasing concentration of dye molecules may affect the adsorbent-based dye removal process. Thus, it is vital to examine the highly concentrated dye molecule in the

adsorption process for dye removal effectiveness by the NZB; determining the q_{\max} of the generated adsorbents is also critical. A batch experiment was carried out to assess the efficiency of an optimum dosage of NZB at various TB concentrations to compute the maximal dye removal from each concentration. Figure 5c illustrates the percentage of dye molecules removed at concentrations ranging from 5 to 30 $\text{mg}\cdot\text{L}^{-1}$. As the TB concentration increased from 5 to 30 $\text{mg}\cdot\text{L}^{-1}$, the dye removal percentage of NZB gradually decreased from 96.5% to 55.1%. The decrease in dye removal percentage was attributed to the NZB surface not having enough active sites or an inadequate adsorbent to adsorb large numbers of TB molecules at increasing concentrations. However, according to Figure 5c, a substantial removal percentage was observed owing to positive charges on the NZB surface caused by intensified driving forces and the diffusion rate of the TB dyes. Figure S4 shows absorbance spectra for various before and after dye concentrations, revealing that increasing the dye concentration increases the absorbance peak after dye adsorption by NZB, which suggests restricting the adsorption at higher concentrations.

3.4. Contact Time

To measure the adsorption rate at various dye concentrations, contact times extending from 0 to 180 min were utilized, since dye molecules may adsorb quickly or slowly on adsorbent surfaces. The optimal dosage of 80 mg of NZB was treated with 25 mL of TB concentrations ranging from 10 to 30 $\text{mg}\cdot\text{L}^{-1}$ to determine the dye removal percentage based on contact time along with natural pH (~4.5–5.0). Figure 5d depicts dye removal percentages vs. contact time at various dye concentrations. Accordingly, NZB removes 10 $\text{mg}\cdot\text{L}^{-1}$ of dye, with 68.8% and 72.0% efficiency during 1 and 30 min. After steadily increasing the dye removal percentage, it reached 93.7% after 60 min of contact, almost reaching saturation. A fast removal of a low-concentration dye from an aqueous solution may be ascribed to the presence of more active sites that may quickly adsorb dye molecules. For 10 $\text{mg}\cdot\text{L}^{-1}$, the minimal contact time is 30 min. At a concentration of 20 $\text{mg}\cdot\text{L}^{-1}$, the influence of time on the adsorbent was evaluated, with contact times up to 180 min. In this batch of contact time, the dye removal percentage for the NZB was 42.4% and 47.0% for 1 and 30 min, respectively. After 60 min, it increased to 73.0% and attained equilibrium. At a TB concentration of 30 $\text{mg}\cdot\text{L}^{-1}$, NZB effectively removed 26.3%, 47.3%, and 55.9% of TB after 1, 30, and 60 min, respectively. After 120 min, it reached 60.2%, and no more improvements were seen. As a result, the removal of TB at low, moderate, and high concentrations takes at least 30, 60, and 120 min, respectively. The optimal amount of adsorbent may absorb dye molecules with a lower concentration than those with higher concentrations; raising the dye concentration to be absorbed by NZB necessitates a longer time need. It should be noted that NZB was able to remove TB efficiently, even at higher concentrations; however, it takes a longer time, as seen with the naked eye through UV-Vis absorbance spectra and supernatant TB solutions after adsorption at different contact times for various dye concentrations. Accordingly, Figure 6 depicts UV-Vis absorbance spectra for the influence of contact time, as well as related photographs of before and after dye adsorption for various dye concentrations. With an increase in the dye concentration, there is an increase in the contact time of the absorbance spectra, indicating that dye adsorption is fast at low concentrations but slow at higher concentrations. The adsorption process for dye concentrations of 10, 20, and 30 $\text{mg}\cdot\text{L}^{-1}$ needs a minimum contact time of 30, 60, and 120 min, as seen in the supernatant solution image.

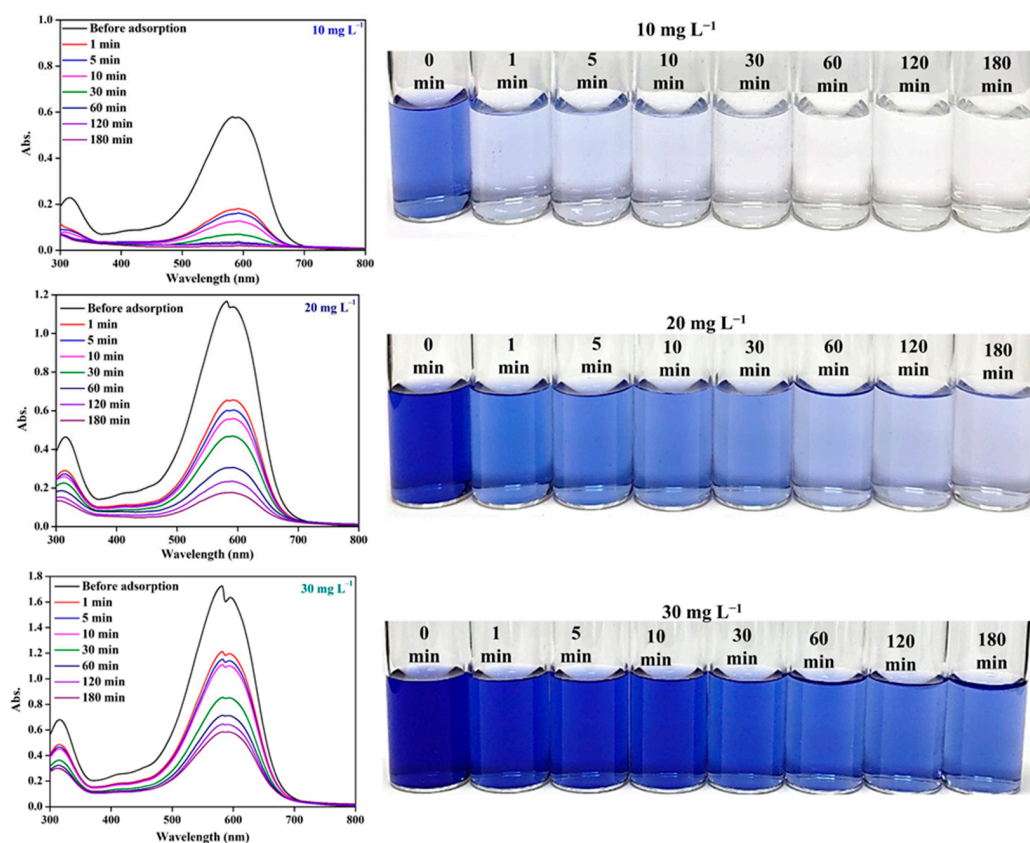


Figure 6. UV-Vis absorption spectra of the contact time before and after TB for dye concentrations of 10, 20, and 30 $\text{mg}\cdot\text{L}^{-1}$ adsorption by NZB LTH with their corresponding photograph of dye supernatants (Dye: TB, dosage: 80 mg, dye concentration: 10–30 $\text{mg}\cdot\text{L}^{-1}$, pH: Natural (~4.5–5.0), volume: 25 mL, temperature: RT).

4. Characterization of the Adsorbent After TB Adsorption

To further understand TB adsorption on NZB surfaces, the adsorbent must be analyzed following dye adsorption by utilizing different characterization approaches. Figure S5a illustrates the N_2 adsorption–desorption BET Type IV isotherm curve, with an inset showing the BJH pore size distribution curve of NZB for porosity measurements (refer to the Supplementary Materials). The typical H3 loop Type IV isotherm curve remained unchanged after dye adsorption; however, the surface area of the NZB was reduced to $9.8 \text{ m}^2\cdot\text{g}^{-1}$. The reduced surface area could be caused by the adsorbed dye particles blocking the pores on the adsorbents' surface. Following dye adsorption, pore volumes decreased while pore diameters increased by $0.0243 \text{ cm}^3\cdot\text{g}^{-1}$ and 6.56 nm , respectively. The decreasing pore volume and increasing pore diameter are due to the dye particles taking up a high place in the pore's depth and the chances of increasing the pore edges through the pore breathing effect [86]. As seen by the diffraction pattern in Figure S5b, dye adsorption weakened and decreased all of the NZB's crystalline peaks, indicating a high likelihood of TB adsorption on the NZB's surface. However, the diffraction pattern showed no other structural changes, suggesting that the adsorbent remained structurally strong after dye adsorption. Moreover, the Raman spectra reveal that the dye adsorption boosted the intensity of the peaks, caused shifts, led to the disappearance of most peaks, and resulted in the formation of new peaks, indicating the potential for dye adsorption on NZB surfaces (Figure S5c). Importantly, the distinctive peaks range from 812 to 836 cm^{-1} and 990 cm^{-1} , respectively, because of the benzene ring vibration and the bending vibration of the aromatic $\text{C}=\text{C}$ structure in the dye. Furthermore, the peak at 1222 cm^{-1} was related to the stretching vibration of $\text{C}-\text{N}$ in the dye structure. The peaks at 1346 and 1424 cm^{-1} were caused by the stretching vibration of $\text{S}=\text{O}$ from sulfonic acid in the dye and the bending vibration of the $-\text{OH}$ group from the TB

dye, respectively. The peak ranging from 1519 to 1577 cm^{-1} was because of the stretching vibration of $-\text{N}=\text{N}-$ in the dye structure [87]. The signal at 1691 cm^{-1} was found to be the bending vibration of the aromatic C-H from the dye structure.

Figure S5d shows the NZB of the IR spectrum following dye absorption, revealing the shifting of peaks and the appearance of new ones. As a result, 3422 and 3256 cm^{-1} appeared due to the dye molecules' $-\text{OH}$ and N-H stretching vibrations, respectively. The stretching vibration of the azo group ($-\text{N}=\text{N}-$) was responsible for the peaks at 1642 and 1550 cm^{-1} . Additionally, the aromatic stretching vibration of $\text{C}=\text{C}$ and the stretching vibration of $-\text{SO}_3^-$ in the dye structure caused characteristic peaks, such as at 1527 and 1349 cm^{-1} . Furthermore, 1326 and 1188 cm^{-1} were claimed to be the stretching vibration of the dye molecule's C-N group. Figure S5e shows FESEM images of NZB following dye treatment at various scales. It was found that the NZB's morphology exhibited irregularities and its surface had become uneven, resulting in the dye molecules settling over the layered structure. Moreover, there were no noticeable changes in the structure or form of the adsorbent surface, suggesting that it remained unchanged, even after the dye was absorbed. Then, XPS was utilized for confirming dye adsorption on NZB surfaces by detecting an extra N 1s peak of dye molecule binding energies at 399.1 and 401.5 eV, which were attributable to $-\text{N}=\text{}$ and $-\text{NH}_2$, respectively (Figure S6). Also, the XPS peaks of Bi 4f shifted from 157.7 and 163.1 eV to 158.3 and 163.6 eV, Ni 2p shifted from 855.0 and 872.7 eV to 855.5 and 873.2 eV, and Zn 2p shifted from 1020.9 and 1044.0 eV to 1021.3 and 1044.5 eV, respectively. This is because dye molecules adsorbed on metals in the LTHs made the binding energies higher.

4.1. Adsorption Isotherm and Kinetics

It is important to determine the q_{max} of an adsorbent by using the Langmuir and Freundlich adsorption isotherms. Additionally, it is vital to determine the kind of adsorption process to understand the dye molecules that are adsorbed on the NZB surfaces. The Langmuir and Freundlich isotherms are linearly fitted in Figure 7a,b, while Table 1 contains the values of the isotherms. The values of the Langmuir and Freundlich isotherms were tabulated using Equations (S1)–(S3) (refer to the Supplementary Materials). Consequently, the q_{max} of NZB is 5.3 $\text{mg}\cdot\text{g}^{-1}$ for the dye concentrations used in this study, ranging from 5 to 30 $\text{mg}\cdot\text{L}^{-1}$. The linear fitting ($R^2 > 0.998$) of the Langmuir isotherm calculated R^2 value was greater than that of the Freundlich isotherm, signifying that the adsorption process could be conducted on a monolayer. The NZB surface exhibited a higher adsorption energy (K_L) for dye molecules, which was determined to be 2.06 $\text{L}\cdot\text{mg}^{-1}$. Equation S2 was employed to calculate the separation factor (R_L), and the value was found to be between 0 and 1, demonstrating that the removal of TB was quite promising for the adsorbent. The adsorbent's $1/n$ value (0.256) was lower than 1, demonstrating that the NZB's surface may exhibit heterogeneity and so can adsorb a substantial quantity of TB dye. Additionally, the Freundlich constant of adsorption capacity (K_F) value was used to determine the quantity of adsorbate adsorbed on adsorbent surfaces, which was 3.02 $\text{mg}\cdot\text{g}^{-1}$. Additionally, the experimental results were validated by the adsorption isotherm models (Figure 7c). The experimental (q_e) consequences for NZB are consistent with the Langmuir model when contrasted with the Freundlich model. This finding suggests that the mechanism of TB adsorption may be a monolayer.

Table 1. Adsorption isotherm findings of NZB LTH after TB adsorption.

Adsorbent	Langmuir				Freundlich		
	q_{max} ($\text{mg}\cdot\text{g}^{-1}$)	K_L ($\text{L}\cdot\text{mg}^{-1}$)	R_L	R^2	$1/n$	K_F ($\text{mg}\cdot\text{g}^{-1}$)	R^2
NZB LTH	5.3	2.06	0.088 to 0.015	0.998	0.256	3.022	0.792

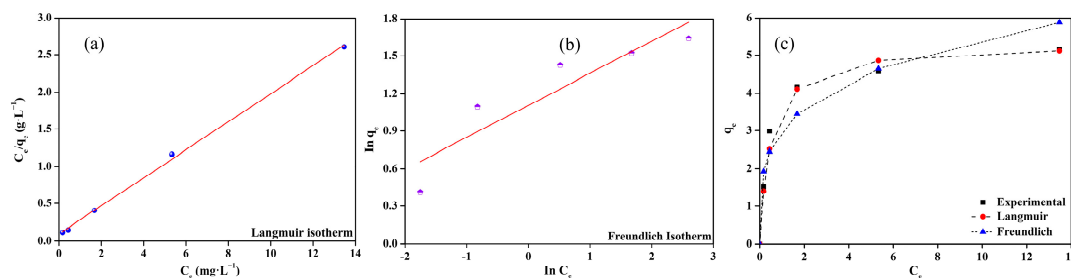


Figure 7. Adsorption isotherm fitting of (a) Langmuir, (b) Freundlich, and (c) Fitting of the experimental q_e data with calculated Langmuir and Freundlich q_e values of the NZB LTH for the TB removal.

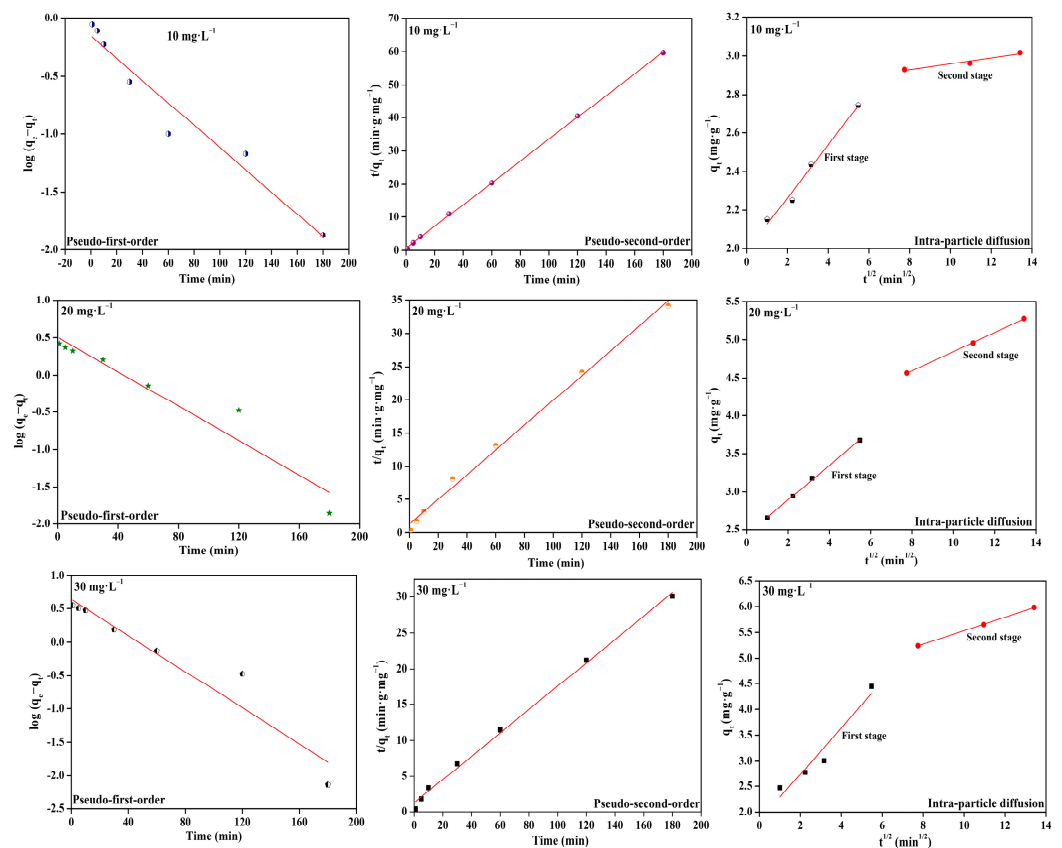
Kinetic studies are essential for the identification of adsorption models and the comprehension of the adsorption process's rate. This study used Equations (S4)–(S7) to analyze the pseudo-first-order and pseudo-second-order models, and intraparticle diffusion (refer to the Supplementary Materials). Adsorption kinetics linear plots for TB concentrations of 10, 20, and 30 mg L^{-1} are depicted in Figure 8. Table 2 indicates that the rate of adsorption studies for all dye concentrations follows pseudo-second-order. This is because the experimental q_e value of all dye concentrations was matched with the calculated q_e value using pseudo-second-order when compared to pseudo-first-order. Moreover, the R^2 value of the correlation coefficient for the pseudo-second-order was greater than that for the pseudo-first-order. Consequently, these findings suggest that the adsorption of TB from water onto NZB is followed by a pseudo-second-order kinetic model [88]. Table 3 depicts the results of Weber's intraparticle diffusion, which was employed to ascertain the dye adsorption rate. The diffusion process is divided into two stages, as illustrated in Figure 8. The initial stage is responsible for the movement of dye molecules from the solution to the adsorbent surface, while the second stage is responsible for the diffusion of particles into the surface pores of the NZB. The intra-particle diffusion rate constants $K_{\text{int}1}$ and $K_{\text{int}2}$ are high and low for the first and second stages, respectively, for all dye concentrations. This is a result of the high driving force of dye molecules in water at the beginning of the process, which decreases to a low level at the end of the process on the pores of the NZB surfaces. Nevertheless, the $K_{\text{int}1}$ and $K_{\text{int}2}$ values are elevated as a result of the increased propelling forces of dye molecules in the water toward the pores of the adsorbent, which is a result of the concentration increase from 10 to 30 mg L^{-1} . Additionally, the gradual increase in the thickness of the dye particle's boundary layers on the adsorbent pores from the first stage to the second stage is indicative of the diffusion of dye molecules at low and high concentrations, respectively, as the values for all dye concentrations increase from C_1 to C_2 . The concentration of dye molecules was increased from 10 to 30 mg L^{-1} , which increased the C_1 and C_2 values. This increase in the number of dye molecules contributed to the thickening of the boundary layers on the pores following pore filling. However, the C_1 value decreased for 30 mg L^{-1} , which may be attributed to the low driving force toward the adsorbent's pores at the primary step, as a result of the possibility of agglomerated dye particles at a higher concentration. Consequently, a higher amount of dye particles (30 mg L^{-1}) resulted in a higher thickness of the boundary layer on the adsorbent's surface in comparison to 10 and 20 mg L^{-1} .

Table 2. Adsorption kinetic models with the correlation coefficients of TB adsorption on NZB LTH.

Adsorbent	Pseudo-First-Order					Pseudo-Second-Order		
	C_0 ($\text{mg}\cdot\text{L}^{-1}$)	$q_{e, \text{exp}}$ ($\text{mg}\cdot\text{g}^{-1}$)	K_1 (min^{-1})	$q_{e, \text{cal}}$ ($\text{mg}\cdot\text{g}^{-1}$)	R^2	K_2 ($\text{g}\cdot\text{mg}^{-1}\cdot\text{min}^{-1}$)	$q_{e, \text{cal}}$ ($\text{mg}\cdot\text{g}^{-1}$)	R^2
NZB LTH	10	2.99	0.022	0.70	0.945	0.165	3.03	0.999
	20	4.58	0.026	3.54	0.920	0.026	5.36	0.994
	30	5.16	0.031	4.34	0.912	0.020	6.13	0.996

Table 3. Intraparticle diffusion constants of TB adsorption on NZB LTH.

	1st Stage	2nd Stage	1st Stage	2nd Stage	1st Stage	2nd Stage	
NZB LTH	10 mg·L ⁻¹	K_{int1}	K_{int2}	C_1	C_2	R^2_1	R^2_2
		0.137	0.015	1.989	2.808	0.980	0.905
	20 mg·L ⁻¹	K_{int1}	K_{int2}	C_1	C_2	R^2_1	R^2_2
		0.228	0.124	2.431	3.595	0.997	0.999
	30 mg·L ⁻¹	K_{int1}	K_{int2}	C_1	C_2	R^2_1	R^2_2
		0.449	0.129	1.841	4.235	0.921	0.999

**Figure 8.** Adsorption kinetics at TB concentrations of 10, 20, and 30 mg·L⁻¹ using pseudo-first-order, pseudo-second-order, and intra-particle diffusion models.

4.2. Mechanism

The adsorption mechanism might be used to understand the adsorbent's capacity to adsorb the dye in water. The decrease in surface area of NZB from 17.08 to 9.8 m²·g⁻¹ following dye adsorption occurred because the dye molecules blocked the pores of NZB by either electrostatic or hydrogen bonding. The pore volume (0.0436 to 0.0243 m³·g⁻¹) dropped while the pore diameters (5.9 to 6.56 nm) rose as a result of the pore-filling process during adsorption. Additionally, the pore diameters of the adsorbent increased owing to the pore breathing effect. The adsorption of dye molecules onto the surfaces of NZB may result in a reduction in peak intensity seen in the XRD pattern. The existence of a substantial number of positive charges on the surface of NZB may account for the electrostatic interaction with the negatively charged TB dye, which likely leads to the physisorption phenomenon. Moreover, the adsorption of dye molecules induces changes in the Raman spectra throughout the 600 to 1800 cm⁻¹ region. The observed IR peaks at 3422 and 3256 cm⁻¹ following adsorption may be attributed to the presence of -OH and N-H groups

in the dye molecule. Furthermore, the presence of $-N=N-$, $C=C$, $-SO_3^-$, and $C-N$ in the dye molecules resulted in the appearance of 1642, 1527, 1349, and 1326 cm^{-1} vibrations. The formation of these IR peaks may be attributed to the electrostatic or hydrogen bonding contact between the positively charged surface of NZB surfaces, which consist of metal nodes and hydroxyl groups. Following the adsorption of dye, the high-resolution spectrum of the NZB LTH reveals the presence of the N 1s peak, which is attributed to the existence of nitrogen in the azo and amino groups within the structure of TB. The binding energies of Bi 4f, Ni 2p, and Zn 2p elements were enhanced upon adsorption, as a result of dye molecules being absorbed onto NZB surfaces. This enhancement could be due to electrostatic interactions between the dye's $-SO_3^-$ groups and the NZB's metal nodes. As seen in Figure 9, the primary mechanism of dye adsorption by the NZB involves a hydrogen bonding contact between the $-OH^+$ groups of the NZB and the sulfonate groups ($-SO_3^-$), amino groups ($-NH_2$), hydroxyl groups ($-OH$), and azo groups ($-N=N-$) of TB. On the other hand, the metal ions present in the surface LTHs, such as Ni^{2+} , Zn^{2+} , and Bi^{3+} , may be electrostatically attracted to the negatively charged $-SO_3^-$ group in the dye structure. As a result, the adsorption process implies that NZB LTH and Trypan blue dye may bind together, enhancing their effectiveness in water remediation via hydrogen bonding and electrostatic interaction.

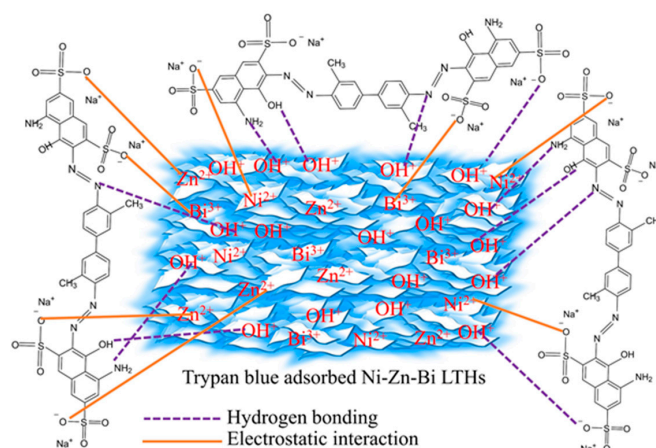


Figure 9. The possible mechanism of Trypan blue (TB) adsorption on the surfaces of NZB LTH.

4.3. Selectivity

It is critical to investigate dye removal from different anionic and cationic dye mixtures using an adsorbent to determine whether or not it is capable of removing additional dyes or simply the specified dye for industrial applications. To this extent, 100 mg of NZB LTH was employed to remove anionic dyes, including Eriochrome black T (EBT), Rose Bengal (RB), Methyl orange (MO), Congo red (CR), and Amido black 10B (AB), as well as cationic dyes, including Safranin O (SO), Crystal violet (CV), Rhodamine 6B (Rh6B), Methylene blue (MB), Brilliant green (BG), and Rhodamine 6G (Rh6G), from a mixture of 18 $\text{mg}\cdot\text{L}^{-1}$ concentration of Trypan blue (TB). The chemical structures of these dyes are illustrated in Figure S7 (refer to the Supplementary Materials). Because the absorbance value of 1.058 determined the concentration of TB, each cationic and anionic dye was adjusted to match the absorbance of TB for selectivity experiments. The UV-Vis absorbance spectra before and after adsorption of a variety of anionic (EBT + TB, MO + TB, RB + TB, CR + TB, and AB + TB) and cationic (SO + TB, CV + TB, Rh6B + TB, MB + TB, BG + TB, and Rh6G + TB) dyes with a mixture of TB are illustrated in Figure 10. The absorbance spectra of the dye mixture after adsorption indicate that NZB LTH is capable of selectively removing TB from a mixture of anionic dyes, such as EBT, MO, RB, and AB. Accordingly, EBT, which only has one negatively charged $-SO_3^-$ group, may not be able to attract NZB as quickly as TB, which has four $-SO_3^-$ and two primary amines ($-NH_2$). As a result of the competition between EBT and TB in the aqueous solution, NZB may have high selectivity

for TB. In contrast to the four -SO_3^- groups and two -NH_2 groups in TB, the adsorption of one positively tertiary amine ($\text{-N(CH}_3)_2$) and negatively charged -SO_3^- group in MO dye to the positively charged NZB may be a weak contact via hydrogen bonding and electrostatic interaction. Therefore, in the presence of MO and TB, negatively charged TB attracts NZB more easily than MO. The chemical structure of RB has quite a few negative charges, such as one COO^- and one O^- group. As a consequence of the competition between RB and TB for NZB, TB has a higher adsorption because of its more negatively charged dye. Therefore, when combined with RB, NZB exhibits significant TB selectivity, whereas AB only contains two -SO_3^- and one -NH_2 group. Thus, when AB competes with TB for adsorption on NZB, the interaction via electrostatic and hydrogen bonding may be slower than TB, which has a faster adsorption owing to four negative charges and two amine groups. NZB hence exhibits notable selectivity for TB when combined with AB. The structure of CR includes two -SO_3^- and two -NH_2 groups. Despite having four negative charges and two positive charges, NZB has a significantly higher removed CR than TB. CR may be easier to remove than TB because it has a low molecular weight, stronger driving forces in water, and/or more hydrogen bonds and electrostatic interactions. In instances of cationic dyes containing TB, NZB was able to remove TB while also removing almost all cationic dyes except CV. The structures of cationic dyes like SO, Rh6B, MB, BG, and Rh6G mostly contain positive charge groups like -NH_2 , -N- , and $\text{-N(CH}_3)_2$, and aromatic rings, which form dipole–dipole hydrogen bonds and Yoshida hydrogen bonds with the highly positively charged hydroxyl (-OH^+) groups of NZB. Despite the presence of tertiary amine in CV's structure, it is possible that the combination of CV and TB's larger molecular size inhibits its rapid adsorption on the surface of NZB through hydrogen bonds, resulting in the observation of a higher absorption peak. As a result, anionic TB has no competition with other cationic dyes for adsorption on positively charged NZB. Because of the high reduction in absorbance peaks of cationic dyes with TB following adsorption by NZB, the removal efficiency of the SO, CV, Rh6B, MB, BG, and Rh6G was determined to be 74.0%, 69.7%, 82.1%, 86.2%, 82.8%, and 77.0%, respectively. Figure 11 shows photographs of different anionic and cation dye mixtures with TB before and after adsorption. The absorption spectra indicate that NZB LTH effectively selectively removes TB when mixed with anionic dyes such as EBT, MO, RB, and AB, in contrast to CR. In the combination of TB with cationic dyes, NZB LTH completely removed TB and was also capable of removing almost all cationic dyes. Therefore, the present study has shown that NZB LTH is a viable material for the highly selective removal of TB when combined with an anionic dye mixture. Additionally, it is capable of removing cationic dyes.

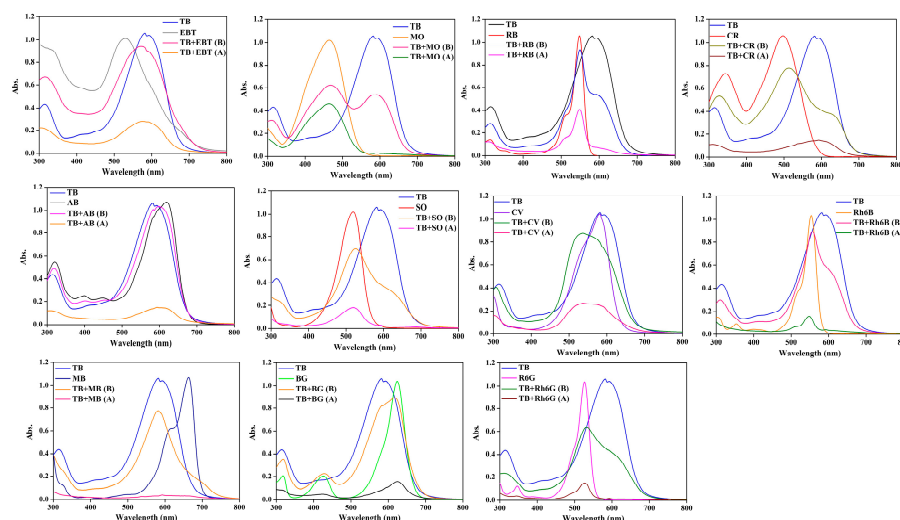


Figure 10. UV-Vis absorbance spectra of TB selectivity using NZB LTH (Dye: TB with other anionic and cationic; Dosage: 100 mg; TB concentration: $18 \text{ mg}\cdot\text{L}^{-1}$; pH: Natural ($\sim 4.5\text{--}5.0$); time: 1 h; volume: 12.5 mL (TB) + 12.5 mL (other dye) and temperature: Room temperature).

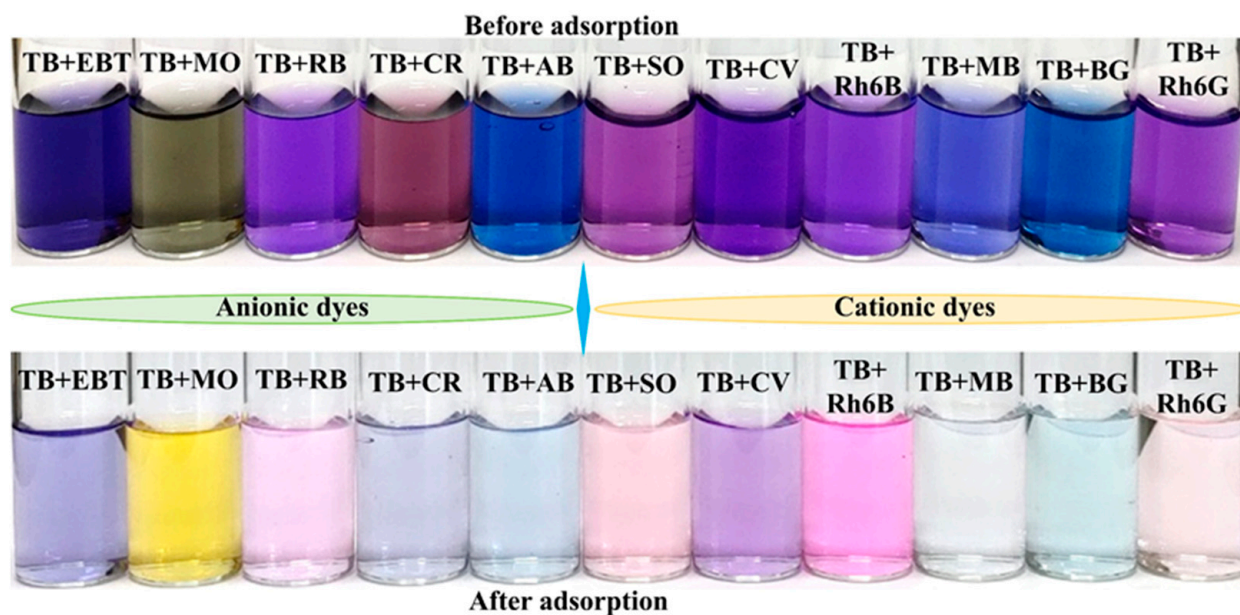


Figure 11. Trypan blue (TB) selectivity with anionic and cationic dyes using NZB LTH.

4.4. Salt Effect

Textiles and other industries that use coloring for products that produce wastewater may contain various types of salt that may affect the efficacy of adsorbents for dye removal using adsorption. As a result, it is critical to determine how the inorganic salts and their higher concentrations affect NZB LTH's dye removal percentage. In this work, sodium sulfate (Na_2SO_4), sodium sulfite (Na_2SO_3), and sodium chloride (NaCl) are the common salts used for TB removal. Figure 12 shows that the experiment without salt had a higher dye removal percentage (73.5%). But when Na_2SO_4 salt was added, the percentage of dye removal dropped to 35.5% at 0.01 M. This was because the negative charges of SO_4^{2-} and SO_3^{2-} in the water caused competition, and the positively charged adsorbent was better at attracting SO_4^{2-} than the SO_3^{2-} group of TB. Furthermore, an increase in salt concentrations from 0.03 M to 0.09 M led to a decrease in the dye removal percentage from 38.4% to 35.1%, primarily due to increased competition from SO_4^{2-} . The addition of Na_2SO_3 to the dye solution resulted in a drastic decrease in the dye removal percentage, reaching 18.0% at a concentration of 0.01 M. This was caused by the salt's high adsorption of the SO_3^{2-} group onto the NZB surfaces, which acted as a shield for TB's SO_3^{2-} group. When compared to Na_2SO_4 , Na_2SO_3 may have a severe effect on the NZB's dye removal percentage. Increasing the salt content from 0.03 M to 0.05 M reduced the dye removal percentage from 17.4% to 10.3%, perhaps because of the NZB's strong attraction to the SO_3^{2-} of salt. Subsequently, the removal percentage increased a little from 11.1% to 11.6% as the concentration was increased from 0.07 M to 0.09 M, mostly due to a higher salt effect. Furthermore, when the concentration of NaCl increased from 0.01 M to 0.09 M, the dye removal percentage increased from 39.7% to 43.1%, which might be attributed to the salt effect, in which the solubility of dye molecules rises with the increasing ion concentration of NaCl in an aqueous solution. Consequently, the percentage of dye removal rose as salt concentration increased. NaCl in the dye solution might therefore have a small effect in comparison to Na_2SO_4 and Na_2SO_3 salts. The UV-Vis absorbance spectra of the different salts' effects on TB adsorption by NZB LTH are shown in Figure 12. These findings demonstrate that as the concentration of salt in the dye solution rises, the high absorbance value could be seen in the following order: $\text{NaCl} < \text{Na}_2\text{SO}_4 < \text{Na}_2\text{SO}_3$.

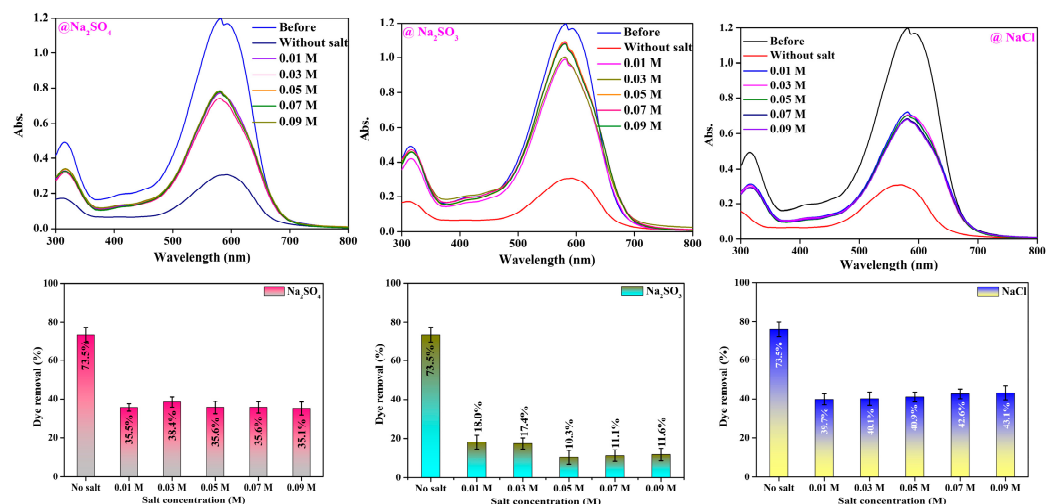


Figure 12. The UV-Vis absorbance spectra of the impact of salts at varying concentrations and their dye removal efficiency in the removal of TB by NZB LTH (Dye: TB; dye concentration: $20 \text{ mg}\cdot\text{L}^{-1}$; Dosage: 80 mg ; pH: Natural ($\sim 4.5\text{--}5.0$); salts: Na_2SO_4 , Na_2SO_3 , and NaCl ; salt concentration: $0.0\text{--}0.09 \text{ M}$; time: 1 h ; volume: 25 mL ; temperature: Room temperature).

4.5. Reusability

Since it saves the energy and cost of the process, the key stage for the adsorption process is the reuse of the adsorbent after adsorption. After TB adsorption by NZB LTH, desorption was obtained by individual contact with 25 mL of methanol, 0.1 M NaOH, and ethanol. A 12 h drying procedure at $60 \text{ }^\circ\text{C}$ was conducted on the NZB LTH in an oven to prepare it for use in the subsequent dye adsorption process after desorption. Similarly, the TB removal treatment was performed five times. As seen in Figure 13d, the NZB removed 82.5% of the dye during the zeroth cycle. The adsorbent then removed a TB percentage ranging from 59.0 to 15.2% , 69.7 to 9.6% , and 56.8 to 25.7% , respectively, using the reagents methanol, ethanol, and 0.1 M NaOH during the first to fifth cycles. The decline in dye removal percentage after each cycle may be attributed to dye molecules taking up permanently in the pores of NZB LTH after the zeroth cycle, as well as a minor loss of adsorbent quantity due to washing after each cycle; thus, increasing the number of cycles corresponds to a decrease in the dye removal percentage. However, when compared to methanol and ethanol, NaOH effectively desorbed TB from the surface of NZB LTH, even after five cycles. Therefore, 0.1 M NaOH proved to be an effective reagent for desorbing TB, allowing for up to three reuses of the NZB LTH. Zubair et al. found similar results when they used various LDHs, such as 0.5 M NaOH, ethanol, and 0.5 M NaOH + NaCl, to desorb EBT dye for up to three cycles [89]. Accordingly, the adsorption capacity of the CoFe, ZnFe, and NiFe LDHs drastically decreased from the first to the third cycles. However, 0.5 M NaOH showed better reusability compared to other agents. The dye molecules' strong adsorption on the adsorbent surfaces through hydrogen bonding or electrostatic interaction may be the cause of their decreasing adsorption capacity or removal efficiency as the number of cycles increases. Another study used water to desorb Coomassie brilliant blue (CBB) from the surfaces of Mg-Cu LDHs; however, after three cycles, this LDH was able to remove 50% of the CBB [90]. Therefore, it might be hard to remove the dye molecules from the LDHs or LTHs using a solvent or water process. To make the process more reusable, it is suggested that other methods be found to remove the dye from the adsorbent surfaces. The UV-Vis absorbance spectra of TB-adsorbed NZB before and after dye adsorption for 0–5 cycles are shown in Figure 13a–c. The absorbance peak becomes higher with each cycle, but the absorbance peaks for 0.1 M NaOH were lower than those for methanol and ethanol when they are used for the recycles.

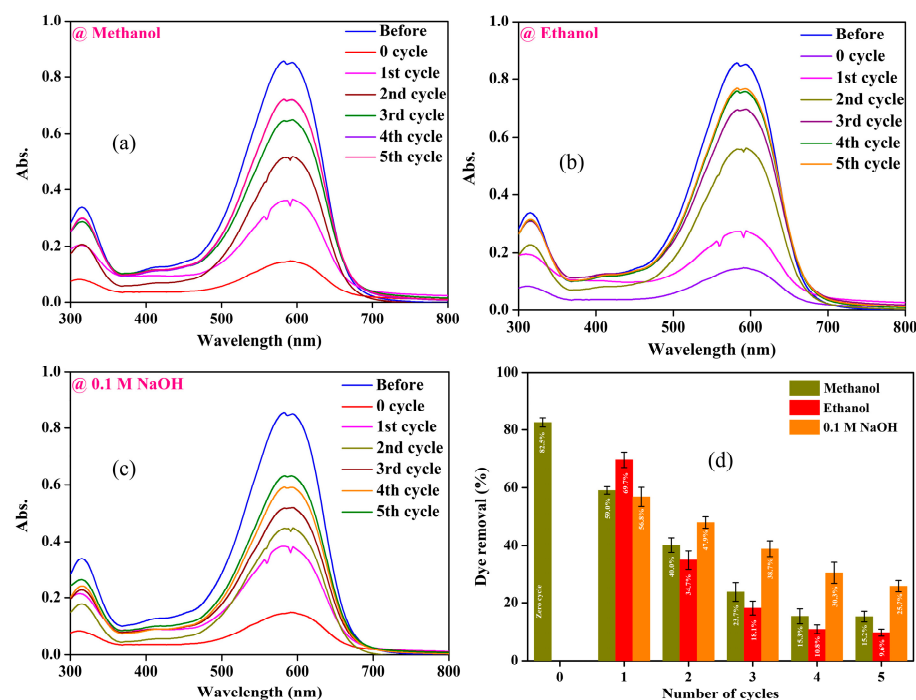


Figure 13. (a–c) UV-Vis absorbance spectra regarding the reusability of NZB LTH before and after TB adsorption (0 to 5 cycles); (d) the calculated dye removal percentage corresponds to the number of cycles. (Dosage: 80 mg, dye concentration: 15 mg·L⁻¹, time: 1 h, pH: Natural (~4.5–5.0), volume: 25 mL, temperature: RT, regenerating agents: methanol, ethanol, and 0.1 M NaOH).

4.6. Comparison

A comparison of the maximum adsorption capacity (q_{\max}) of the adsorbent for dye removal with other reported adsorbents is provided in Table 4. However, comparing the findings of adsorbents with one another may be contrary as various pieces of research utilized different synthesis techniques, adsorbent types, dosages, dye concentrations, pH, volume of the dye solution, etc. In general, the q_{\max} of the adsorbents is contingent upon the concentration of the dye, the volume of the solution, and the dosage. A higher q_{\max} may result in a minimal adsorbent dosage, which is accompanied by a higher solution volume and dye concentration. A lowered q_{\max} may result in a maximal dosage with a lower volume and dye concentration. The q_{\max} of the NZB LTH (5.3 mg·g⁻¹) was lower than that of other adsorbents, as indicated in Table 4. The low value attained in this investigation may be attributed to the use of a high dosage (0.08 g) in a low volume (25 mL) and a low-concentrated dye (5–30 mg·L⁻¹). Typically, the adsorbents, including montmorillonite-modified hexadecyltrimethylammonium bromide and polyethylene glycol (MMT@HTAB@PEG), hydroxyapatite-modified reduced graphene oxide (HA@rGO), zinc nanoparticle-modified luffa sponge (LS-Zn), and magnesium oxide nanoparticles (MgO), were able to achieve a high q_{\max} of 267.3, 146.5, 129.8, and 93.5 mg g⁻¹, respectively, as a result of the higher volume of solution (50 mL). Even so, the adsorbents exhibited a difference in high and low q_{\max} based on the dosage and dye concentrations. Furthermore, the pH 2 used by MMT@HTAB@PEG to remove TB may not be environmentally friendly. Adsorbents like pyrolyzed maple bark (PMB), poly(diallyldimethylammonium chloride)/graphene oxide hydrogel (PDDA/GO), and GO-doped nano-hydroxyapatite (GO-nHAp) had moderate q_{\max} values of 72.5, 50.0, and 41.0 mg g⁻¹, which could be attributed to the low solution volume or concentration of the dye used. NZB LTH has poorer efficacy than the others; however, it has a natural pH (~4.5–5.0), is simple to synthesize, environmentally friendly, and inexpensive. Future research might be conducted to improve its dye removal performance or alternative effective LTHs could be synthesized for the efficient removal of organic dyes.

Table 4. Comparing Ni-Zn-Bi LTH (NZN LTH) to other adsorbents for the removal of Trypan blue (TB).

Adsorbents	Dye	Dye Concentration	pH	Volume (mL)	Dosage (g)	q _{max} (mg·g ⁻¹)	Ref.
MMT@HTAB@PEG	Trypan blue	20–120 mg·L ⁻¹	2.0	50	0.03	267.3	[91]
HA@rGO	Trypan blue	50 mg·L ⁻¹	Natural	50	0.1	146.5	[92]
LS-Zn	Trypan blue	10–200 mg·L ⁻¹	7.0	50	1.0	129.8	[93]
MgO	Trypan blue	15–45 mg·L ⁻¹	5.4	50	0.02	93.5	[94]
PMB	Trypan blue	1000 mg·L ⁻¹	7.5	10	0.1	72.5	[95]
PDDA/GO	Trypan blue	0.001–1 mM	6.0	0.5	0.001	50.0	[96]
GO-nHAp	Trypan blue	50–200 mg·L ⁻¹	6.7	25	0.05	41.0	[97]
NZN LTH	Trypan blue	5–30 mg·L ⁻¹	~4.5–5.0	25	0.08	5.3	This work

5. Materials and Methods

Zinc (II) nitrate hexahydrate (Zn(NO₃)₂·6H₂O, 95.0%), sodium chloride (NaCl, 99.0%), sodium hydroxide (NaOH, 93.0%), hydrochloric acid (HCl, 35–37%), and sodium sulfate anhydrous (Na₂SO₄, 99.0%) were obtained from Duksan pure chemicals Co., Ltd., Ansan-si, Republic of Korea. Nickel (II) nitrate hexahydrate (Ni(NO₃)₂·6H₂O, 97.0%), Bismuth (III) nitrate pentahydrate (Bi(NO₃)₃·5H₂O, 98.0%), and TB dye (Figure S1) were obtained from Daejung chemicals & metals Co., Ltd., Siheung-si, Republic of Korea. Sodium sulfite anhydrous (Na₂SO₃, 95.0%) was received from DC Chemicals Co., Ltd., Shanghai, China. The chemicals used in this study were utilized without any additional purification steps.

5.1. Synthesis of NiZnBi LTH (NZN LTH or NZB)

NZN was produced via the co-precipitation process. Initially, 0.1 M Ni(NO₃)₂·6H₂O, 0.05 M Zn(NO₃)₂·6H₂O, and 0.025 M Bi(NO₃)₃·5H₂O were added to 100 mL of purified water, which was then stirred for 30 min to ensure that all of the substances were completely dissolved. However, due to the insoluble nature of Bi(NO₃)₃·5H₂O in water, a series of drops of concentrated HCl was introduced into the mixture solution to solubilize it. Then, to achieve a precipitate, 1.0 M NaOH was added slowly to the above solutions to bring them to a pH of 10. The solution, which had been adjusted for pH, was constantly stirred at 60 °C for 12 h. Subsequently, the particulates were immersed in the solution using purified water until the pH leveled at 7.0. This process aided in the purification of the samples by removing any excess NaOH. Subsequently, the purified particles were dried in an oven at 60 °C to acquire the NZB. Furthermore, batch adsorption and characterization investigations were performed utilizing the acquired NZB.

5.2. Batch Adsorption Study

An experiment on batch adsorption was conducted using concentrations of Trypan blue (TB) ranging from 5 to 30 mg·L⁻¹. The batch adsorption at room temperature included testing different parameters, including pH, adsorbent dosage, initial dye concentration, and time. The pH of the dye solution was varied using 1 M NaOH and 1 M HCl to explore the effect of pH. To study TB adsorption, 80 mg of NZB was added to 25 mL of various TB solution concentrations in a 100 mL conical flask. The flasks were then placed in a shaking bath and left to shake for 1 h. After that, the NZB that had adsorbed TB was isolated from the dye solution using 10 min centrifugation at 3000 rpm. The supernatant collected thereafter was used to assess the efficiency of NZB in removing TB by a calibration plot at λ_{max} 590 nm. The following Equations (1) and (2) were employed to calculate the removal percentage (R%) and adsorption capacity (q_e (mg·g⁻¹)) of TB. The TB removal performance was analyzed in triplicate for each parameter influence to calculate standard errors.

$$R\% = \frac{C_i - C_f}{C_i} \times 100 \quad (1)$$

where C_i and C_f are the dye concentrations before and after adsorption, respectively.

$$q_e \left(\text{mg} \cdot \text{g}^{-1} \right) = \frac{C_i - C_f}{M} \times V \quad (2)$$

where V is the dye solution in liters (L) and M is the adsorbent mass in grams (g).

5.3. Characterization Techniques

X-ray diffraction (XRD) with an X'Pert PRO from PANalytical, Almelo, Netherlands, was used to analyze the structural stability of the adsorbents before and after NZB dye adsorption. The scan category applied was 'Continuous', with a scan rate of 5° min^{-1} and scan range and step size of analysis of $10\text{--}80^\circ$ and 0.026, respectively. The functional groups of adsorbents between wavenumbers of 650 and 4000 cm^{-1} were analyzed by Fourier transform-infrared spectroscopy-attenuated total reflection (FTIR-ATR) using QATR-S, Shimadzu, Kyoto, Japan. The adsorbent surface area was studied at 77 K using Micromeritics, 3-FLEX, Norcross, GA, USA, and porosity was measured using the Barrett-Joyner-Halenda (BJH) method. The morphology and elemental composition and mapping of NZB were analyzed by field-emission scanning electron microscope (FESEM, S-4800, Hitachi, Tokyo, Japan) and energy dispersive X-ray spectrometer (EDX, Horiba EMAX, Horiba Co., Ltd., Kyoto, Japan), respectively. X-ray photoelectron spectroscopy (XPS, AXIS ULTRA DLD, Kratos Analytical instrument, Manchester, UK) using a monochromatic light source (Al K alpha) was utilized to study the oxidation states of elements in the NZB, and The XPS-PEAK41, Version 4.1, a free software developed by Raymond W.M. Kwok at The Chinese University of Hong Kong in Shatin, Hong Kong, was employed to conduct XPS peak fitting. The initial and final dye concentrations were analyzed using a UV-Vis spectrophotometer (Ubi-1800, MicroDigital Co., Ltd., Seongnam-si, Republic of Korea). This study used the shaking bath model JSSI-070T, 63L capacity, JS Research Co., Ltd., Gongju-si, Republic of Korea, for adsorption studies.

6. Conclusions

This study used co-precipitation to synthesize Ni-Zn-Bi LTH (NZB) for the removal of Trypan blue (TB) from water. The physiochemical characteristics of NZB were investigated both before and following dye adsorption using a variety of techniques. The dye solution's natural pH ($\sim 4.5\text{--}5.0$) was used for all adsorption experiments, and the q_{max} of NZB was calculated to be 5.3 mg g^{-1} using the Langmuir model. Regarding selectivity, NZB is very effective at removing anionic dyes and completely removes cationic dyes when combined with TB. Studies found that increasing the salt concentration (0.01–0.09 M) of Na_2SO_3 reduced TB removal compared to NaCl and Na_2SO_4 . The removal efficiency of TB is 15.2%, 9.6%, and 25.7%, respectively, as a result of the reusability of NZB in methanol, ethanol, and NaOH reagents for five cycles. Based on the experiments, NZB LTH may be able to remove cationic or anionic dyes via surface modification of incompatible materials. The findings show that NZB LTH might be a promising material for removing TB and a variety of anionic and cationic dyes, with probable applications in the treatment of dye-based industrial effluent.

Supplementary Materials: The following supporting information can be downloaded at: <https://www.mdpi.com/article/10.3390/inorganics12110296/s1>, Figure S1: Chemical structure of Trypan blue (TB) dye; Figure S2: UV-Vis absorption spectra of the TB's solution at different pHs and effect of pHs such as 2, 4, natural ($\sim 4.5\text{--}5.0$), 6, 8, and 10 for before and after dye adsorption by NZB LTH (Dye: Trypan Blue (TB), Concentration: $15 \text{ mg} \cdot \text{L}^{-1}$, Dosage: 80 mg, Volume: 25 mL, Time: 1 h, Temperature: Room temperature (RT)); Figure S3: UV-Vis absorption spectra of the adsorbent dosage (10–80 mg) for before and after TB adsorption by NZB (Dye: TB, pH: Natural ($\sim 4.5\text{--}5.0$), Concentration: $10 \text{ mg} \cdot \text{L}^{-1}$, Volume: 25 mL, Time: 1 h, Temperature: RT); Figure S4: UV-Vis absorption spectra of the effect of initial dye concentration ($5\text{--}30 \text{ mg L}^{-1}$) for before and after TB adsorption by NZB (Dye: TB, Dosage: 80 mg, pH: Natural ($\sim 4.5\text{--}5.0$), Time: 1 h, Volume: 25 mL, Temperature: RT); Figure S5: Characterizing NZB after TB adsorption: (a) N_2 adsorption-desorption isotherm and BJH pore size

distribution; (b) XRD pattern; (c) Raman spectrum; (d) FTIR-ATR spectrum; and (e) FESEM images at 5 and 1 μm scales; Figure S6: Characterizing NZB after TB adsorption: XPS full survey spectrum and high-resolution spectra of Bi 4f, C 1s, O 1s, Ni 2p, Zn 2p, and N 1s; Adsorption Isotherms and Kinetic Studies; Figure S7: Chemical structure of organic dyes.

Author Contributions: Conceptualization, G.S. and K.D.; methodology, G.S.; software, M.A.; validation, N.B. and M.A.; formal analysis, K.S. and T.S.; investigation, G.S.; resources, N.B.; data curation, N.B. and K.S.; writing—original draft preparation, G.S.; writing—review and editing, K.D. and T.H.O.; visualization, M.A.; supervision, T.H.O.; project administration, T.H.O.; funding acquisition, T.H.O. All authors have read and agreed to the published version of the manuscript.

Funding: This research was funded by the National Research Foundation of Korea (NRF) by the Korean Government (MSIT), grant no: 2022R1A2C100428.

Data Availability Statement: The original contributions presented in the study are included in the article/Supplementary Materials, further inquiries can be directed to the corresponding authors.

Conflicts of Interest: The authors declare no conflicts of interest.

References

1. Abu Elella, M.H.; Aamer, N.; Abdallah, H.M.; López-Maldonado, E.A.; Mohamed, Y.M.A.; El Nazer, H.A.; Mohamed, R.R. Novel high-efficient adsorbent based on modified gelatin/montmorillonite nanocomposite for removal of malachite green dye. *Sci. Rep.* **2024**, *14*, 1228. [[CrossRef](#)] [[PubMed](#)]
2. Zulkiflee, A.; Mansoob Khan, M.; Yusuf Khan, M.; Khan, A.; Hilni Harunsani, M. Nb₂O₅/BiOCl composite as a visible-light-active photocatalyst for the removal of RhB dye and photoelectrochemical studies. *J. Photochem. Photobiol. A* **2024**, *446*, 115177. [[CrossRef](#)]
3. Sriram, G.; Thangarasu, S.; Selvakumar, K.; Kurkuri, M.; Dhineshababu, N.R.; Oh, T.H. Effective removal of Rose Bengal using Ni-Co-Zn layered triple hydroxide: Studies on batch adsorption, mechanism, selectivity, co-ions, and reusability. *Colloids Surf. A Physicochem. Eng. Asp.* **2024**, *685*, 133199. [[CrossRef](#)]
4. Varjani, S.; Rakholiya, P.; Shindhal, T.; Shah, A.V.; Ngo, H.H. Trends in dye industry effluent treatment and recovery of value added products. *J. Water Process Eng.* **2021**, *39*, 101734. [[CrossRef](#)]
5. Slama, H.B.; Chenari Bouket, A.; Pourhassan, Z.; Alenezi, F.N.; Silini, A.; Cherif-Silini, H.; Oszako, T.; Luptakova, L.; Golińska, P.; Belbahri, L. Diversity of Synthetic Dyes from Textile Industries, Discharge Impacts and Treatment Methods. *Appl. Sci.* **2021**, *11*, 6255. [[CrossRef](#)]
6. Louis, K.S.; Siegel, A.C. Cell Viability Analysis Using Trypan Blue: Manual and Automated Methods. In *Mammalian Cell Viability: Methods and Protocols*; Stoddart, M.J., Ed.; Humana Press: Totowa, NJ, USA, 2011; pp. 7–12. [[CrossRef](#)]
7. Abdelkader, E.A.; McBain, V.A.; Anand, M.; Scott, N.W.; Rehman Siddiqui, M.A.; Lois, N. In vivo safety of trypan blue use in vitreoretinal surgery. *Retina* **2011**, *31*, 1122–1127. [[CrossRef](#)] [[PubMed](#)]
8. Dutta, S.; Gupta, B.; Srivastava, S.K.; Gupta, A.K. Recent advances on the removal of dyes from wastewater using various adsorbents: A critical review. *Mater. Adv.* **2021**, *2*, 4497–4531. [[CrossRef](#)]
9. Hussain, B.; Sajad, M.; Usman, H.; Al-Ghanim, K.A.; Riaz, M.N.; Berenjian, A.; Mahboob, S.; Show, P.L. Assessment of hepatotoxicity and nephrotoxicity in Cirrhinus mrigala induced by trypan blue—An azo dye. *Environ. Res.* **2022**, *215*, 114120. [[CrossRef](#)]
10. Ledakowicz, S.; Paździor, K. Recent Achievements in Dyes Removal Focused on Advanced Oxidation Processes Integrated with Biological Methods. *Molecules* **2021**, *26*, 870. [[CrossRef](#)]
11. Katheresan, V.; Kannedo, J.; Lau, S.Y. Efficiency of various recent wastewater dye removal methods: A review. *J. Environ. Chem. Eng.* **2018**, *6*, 4676–4697. [[CrossRef](#)]
12. Sriram, G.; Bendre, A.; Mariappan, E.; Altalhi, T.; Kigga, M.; Ching, Y.C.; Jung, H.-Y.; Bhaduri, B.; Kurkuri, M. Recent trends in the application of metal-organic frameworks (MOFs) for the removal of toxic dyes and their removal mechanism—A review. *Sustain. Mater. Technol.* **2022**, *31*, e00378. [[CrossRef](#)]
13. Bharathiraja, B.; Jayamuthunagai, J.; Praveenkumar, R.; Iyyappan, J. Phytoremediation Techniques for the Removal of Dye in Wastewater. In *Bioremediation: Applications for Environmental Protection and Management*; Varjani, S.J., Agarwal, A.K., Gnansounou, E., Gurunathan, B., Eds.; Springer: Singapore, 2018; pp. 243–252. [[CrossRef](#)]
14. Zafar, A.M.; Naem, A.; Minhas, M.A.; Hasan, M.J.; Rafique, S.; Ikhlaiq, A. Removal of reactive dyes from textile industrial effluent using electrocoagulation in different parametric conditions of aluminum electrodes. *Total Environ. Adv.* **2024**, *9*, 200087. [[CrossRef](#)]
15. Madhurima, V.P.; Kumari, K.; Jain, P.K. Synthesis and study of carbon nanomaterials through arc discharge technique for efficient adsorption of organic dyes. *Diam. Relat. Mater.* **2024**, *141*, 110538. [[CrossRef](#)]
16. Uğan, M.; Onac, C.; Kaya, A.; Köseoğlu, D.; Akdoğan, A. Removal of Reactive Red 195 dye from textile industry wastewater with Deep Eutectic Solvent-based green extraction. *J. Mol. Liq.* **2024**, *398*, 124249. [[CrossRef](#)]
17. Le Nam Vo, V.; Chung, Y.-M. Catalytic wet peroxide oxidation of organic dye with in-situ generated H₂O₂ over bifunctional Fe-Pt@Pd/SiO₂ catalyst prepared by double-metal complex salt approach. *Appl. Catal. A* **2024**, *676*, 119640. [[CrossRef](#)]

18. Cigeroğlu, Z.; El Messaoudi, N.; Şenol, Z.M.; Başkan, G.; Georgin, J.; Gubernat, S. Clay-based nanomaterials and their adsorptive removal efficiency for dyes and antibiotics: A review. *Mater. Today Sustain.* **2024**, *26*, 100735. [[CrossRef](#)]
19. Modwi, A.; Elamin, M.R.; Abdulkhair, B.Y.; Elamin, N.Y.; Ali Ben Aissa, M.; Ben Said, R. Synthesis and characterization of Ti-doped $Y_2O_3@C_3N_4$ nanocomposite for the removal of dyes from aqueous solution. *Inorg. Chem. Commun.* **2023**, *158*, 111594. [[CrossRef](#)]
20. Rimzim; Singh, J.; Mittal, S.; Singh, H. Robust removal of cationic dyes by zinc ferrite composites in single and ternary dye systems. *Inorg. Chem. Commun.* **2023**, *153*, 110756. [[CrossRef](#)]
21. Rath, B.S.; Kumar, P.S. Application of adsorption process for effective removal of emerging contaminants from water and wastewater. *Environ. Pollut.* **2021**, *280*, 116995. [[CrossRef](#)]
22. Velicu, M.; Fu, H.; Suri, R.P.S.; Woods, K. Use of adsorption process to remove organic mercury thimerosal from industrial process wastewater. *J. Hazard. Mater.* **2007**, *148*, 599–605. [[CrossRef](#)]
23. Papić, S.; Koprivanac, N.; Lončarić Božić, A.; Meteš, A. Removal of some reactive dyes from synthetic wastewater by combined Al(III) coagulation/carbon adsorption process. *Dye. Pigment.* **2004**, *62*, 291–298. [[CrossRef](#)]
24. Gonçalves, J.O.; Strieder, M.M.; Silva, L.F.O.; dos Reis, G.S.; Dotto, G.L. Advanced technologies in water treatment: Chitosan and its modifications as effective agents in the adsorption of contaminants. *Int. J. Biol. Macromol.* **2024**, *270*, 132307. [[CrossRef](#)] [[PubMed](#)]
25. Liu, P.; Wu, L.; Guo, Y.; Huang, X.; Guo, Z. High crystalline LDHs with strong adsorption properties effectively remove oil and micro-nano plastics. *J. Clean. Prod.* **2024**, *437*, 140628. [[CrossRef](#)]
26. Sarkar, A.; Mushahary, N.; Basumatary, F.; Das, B.; Basumatary, S.F.; Venkatesan, K.; Selvaraj, M.; Rokhum, S.L.; Basumatary, S. Efficiency of montmorillonite-based materials as adsorbents in dye removal for wastewater treatment. *J. Environ. Chem. Eng.* **2024**, *12*, 112519. [[CrossRef](#)]
27. Tsoutsas, E.K.; Tolkou, A.K.; Kyzas, G.Z.; Katsoyiannis, I.A. An Update on Agricultural Wastes Used as Natural Adsorbents or Coagulants in Single or Combined Systems for the Removal of Dyes from Wastewater. *Water Air Soil Pollut.* **2024**, *235*, 178. [[CrossRef](#)]
28. Akash, S.; Rameshwar, S.S.; Rajamohan, N.; Rajasimman, M.; Vo, D.-V.N. Metal oxide nanobiochar materials to remediate heavy metal and dye pollution: A review. *Environ. Chem. Lett.* **2024**, *22*, 2091–2112. [[CrossRef](#)]
29. Njuguna, D.; Schönherr, H. Tunable Gellan Gum Hydrogels as High Capacity Adsorbents for Rapid Dye Removal. *ACS Appl. Polym. Mater.* **2024**, *6*, 1528–1539. [[CrossRef](#)]
30. Yuan, Z.; Li, F.; Zhang, X.; Li, M.-C.; Chen, Y.; Hoop, C.F.d.; Qi, J.; Huang, X. Bio-based adsorption foam composed of MOF and polyethyleneimine-modified cellulose for selective anionic dye removal. *Environ. Res.* **2024**, *248*, 118263. [[CrossRef](#)]
31. Tamer, T.M.; Abbas, R.; Sadik, W.A.; Omer, A.M.; Abd-Ellatif, M.M.; Mohy-Eldin, M.S. Development of novel amino-ethyl chitosan hydrogel for the removal of methyl orange azo dye model. *Sci. Rep.* **2024**, *14*, 1284. [[CrossRef](#)]
32. Koli, A.; Kumar, A.; Pattanshetti, A.; Supale, A.; Garadkar, K.; Shen, J.; Shaikh, J.; Praserttham, S.; Motkuri, R.K.; Sabale, S. Hierarchical Porous Activated Carbon from Wheat Bran Agro-Waste: Applications in Carbon Dioxide Capture, Dye Removal, Oxygen and Hydrogen Evolution Reactions. *ChemPlusChem* **2024**, *89*, e202300373. [[CrossRef](#)]
33. Koli, A.; Battu, A.K.; Motkuri, R.K.; Sabale, S. Hierarchical porous activated carbon derived from agro-waste for potential CO₂ capture and efficient dye removal applications. *Biomass Convers. Biorefinery* **2024**, *14*, 10177–10188. [[CrossRef](#)]
34. Bagherzadeh, M.; Salehi, G.; Rabiee, N. Rapid and efficient removal of methylene blue dye from aqueous solutions using extract-modified Zn–Al LDH. *Chemosphere* **2024**, *350*, 141011. [[CrossRef](#)] [[PubMed](#)]
35. Karim, A.R.; Danish, M.; Alam, M.G.; Majeed, S.; Alanazi, A.M. A review of pre- and post-surface-modified neem (*Azadirachta indica*) biomass adsorbent: Surface functionalization mechanism and application. *Chemosphere* **2024**, *351*, 141180. [[CrossRef](#)] [[PubMed](#)]
36. Wu, X.; Wu, D.; Fu, R.; Zeng, W. Preparation of carbon aerogels with different pore structures and their fixed bed adsorption properties for dye removal. *Dye. Pigment.* **2012**, *95*, 689–694. [[CrossRef](#)]
37. Wu, C.; Li, K.; Ni, X.; He, Y.; Wang, Y.; Ju, A. Efficient Template-Catalyzed In Situ Polymerization for Carbon Xerogels with Large Specific Surface Area and High Adsorption. *Langmuir* **2024**, *40*, 9985–9992. [[CrossRef](#)]
38. Kazemi, S.Y.; Pourfaraj, R.; Biparva, P. Synthesis of MgZnAl Layered Triple Hydroxide Nanoplates as an Efficient Adsorbent for Removing the Acid Yellow 76 Azo Dye. *ChemistrySelect* **2024**, *9*, e202400789. [[CrossRef](#)]
39. Singh, V.K.; Sett, A.; Karmakar, S. Waste to wealth: Facile activation of red mud waste and insights into industrial reactive dye removal from wastewater. *Chem. Eng. J.* **2024**, *481*, 148373. [[CrossRef](#)]
40. Noormohammadi, M.; Zabihi, M.; Faghihi, M. Novel chitosan–clay–iron nanocomposites supported on anodic aluminum as an efficient plate-shaped adsorbent for the removal of arsenic and dye from aqueous solutions. *J. Phys. Chem. Solids* **2024**, *187*, 111874. [[CrossRef](#)]
41. Wei, S.; Tan, Z.; Liu, Z.; Zuo, H.; Xia, Y.; Zhang, Y. Removal of methyl orange dye by high surface area biomass activated carbon prepared from bamboo fibers. *Ind. Crops Prod.* **2024**, *218*, 118991. [[CrossRef](#)]
42. Wang, A.-L.; Xu, H.; Li, G.-R. NiCoFe Layered Triple Hydroxides with Porous Structures as High-Performance Electrocatalysts for Overall Water Splitting. *ACS Energy Lett.* **2016**, *1*, 445–453. [[CrossRef](#)]

43. Bahadi, S.A.; Drmosh, Q.A.; Onaizi, S.A. Synergism between polyethyleneimine, graphene oxide, and MgFeAl-layered triple hydroxide in removing acid red 1 dye and bisphenol A from contaminated water samples. *Colloids Surf. A Physicochem. Eng. Asp.* **2024**, *688*, 133579. [[CrossRef](#)]
44. Mahmoud, R.; Kotb, N.M.; Gadelhak, Y.; El-Ela, F.I.A.; Shehata, A.Z.; Othman, S.I.; Allam, A.A.; Rudayni, H.A.; Zaher, A. Investigation of ternary Zn–Co–Fe layered double hydroxide as a multifunctional 2D layered adsorbent for moxifloxacin and antifungal disinfection. *Sci. Rep.* **2024**, *14*, 806. [[CrossRef](#)] [[PubMed](#)]
45. Mittal, J. Recent progress in the synthesis of Layered Double Hydroxides and their application for the adsorptive removal of dyes: A review. *J. Environ. Manag.* **2021**, *295*, 113017. [[CrossRef](#)]
46. Daud, M.; Hai, A.; Banat, F.; Wazir, M.B.; Habib, M.; Bharath, G.; Al-Harhi, M.A. A review on the recent advances, challenges and future aspect of layered double hydroxides (LDH)—Containing hybrids as promising adsorbents for dyes removal. *J. Mol. Liq.* **2019**, *288*, 110989. [[CrossRef](#)]
47. Shan, R.; Yan, L.; Yang, K.; Yu, S.; Hao, Y.; Yu, H.; Du, B. Magnetic Fe₃O₄/MgAl-LDH composite for effective removal of three red dyes from aqueous solution. *Chem. Eng. J.* **2014**, *252*, 38–46. [[CrossRef](#)]
48. Asadi, E.; Haroonian, P.; Ghaedi, M.; Asfaram, A. Removal of tartrazine and indigo carmine with layered double hydroxide-modified graphite nanocomposite: Isotherm, kinetics and response surface methodology (RSM) optimization. *J. Mol. Liq.* **2024**, *402*, 124769. [[CrossRef](#)]
49. Gupta, V.; Gupta, S.; Miura, N. Electrochemically synthesized large area network of CoxNiyAlz layered triple hydroxides nanosheets: A high performance supercapacitor. *J. Power Sources* **2009**, *189*, 1292–1295. [[CrossRef](#)]
50. Patil, K.; Babar, P.; Bae, H.; Jo, E.; Jang, J.S.; Bhoite, P.; Kolekar, S.; Kim, J.H. Enhanced electrocatalytic activity of a layered triple hydroxide (LTH) by modulating the electronic structure and active sites for efficient and stable urea electrolysis. *Sustain. Energy Fuels* **2022**, *6*, 474–483. [[CrossRef](#)]
51. Hamad, H.A.; Nageh, H.; El-Bery, H.M.; Kasry, A.; Carrasco-Marín, F.; Elhady, O.M.; Soliman, A.M.M.; El-Remaily, M.A.E.A.A.A. Unveiling the exceptional synergism-induced design of Co-Mg-Al layered triple hydroxides (LTHs) for boosting catalytic activity toward the green synthesis of indol-3-yl derivatives under mild conditions. *J. Colloid Interface Sci.* **2021**, *599*, 227–244. [[CrossRef](#)]
52. Khatun, S.; Roy, P. Cobalt chromium vanadium layered triple hydroxides as an efficient oxygen electrocatalyst for alkaline seawater splitting. *Chem. Commun.* **2022**, *58*, 1104–1107. [[CrossRef](#)]
53. Kandasamy, B.; Govindasamy, P.; Thangavelu, P.; Theerthagiri, J.; Min, A.; Choi, M.Y. Improved visible light photocatalytic degradation of yttrium doped NiMgAl layered triple hydroxides for the effective removal of methylene blue dye. *Chemosphere* **2022**, *290*, 133299. [[CrossRef](#)] [[PubMed](#)]
54. Ismail, U.M.; Onaizi, S.A.; Vohra, M.S. Novel MgCuAl-layered triple hydroxide for aqueous selenite and selenate treatment. *Emergent Mater.* **2024**, *7*, 521–532. [[CrossRef](#)]
55. Chowdhury, M.F.; Kim, C.-M.; Jang, A. High-efficient and rapid removal of anionic and cationic dyes using a facile synthesized sole adsorbent NiAlFe-layered triple hydroxide (LTH). *Chemosphere* **2023**, *332*, 138878. [[CrossRef](#)] [[PubMed](#)]
56. Gao, Y.; Zhang, T.; Mao, Y.; Wang, J.; Sun, C. Highly efficient bifunctional layered triple Co, Fe, Ru hydroxides and oxides composite electrocatalysts for Zinc-Air batteries. *J. Electroanal. Chem.* **2023**, *935*, 117315. [[CrossRef](#)]
57. Sriram, G.; Dhanabalan, K.; Ajeya, K.V.; Aruchamy, K.; Ching, Y.C.; Oh, T.H.; Jung, H.-Y.; Kurkuri, M. Recent progress in anion exchange membranes (AEMs) in water electrolysis: Synthesis, physio-chemical analysis, properties, and applications. *J. Mater. Chem. A* **2023**, *11*, 20886–21008. [[CrossRef](#)]
58. Wang, G.; He, L.; Guo, Z.; Li, M. Ternary metal layered hydroxides: As promising electrode materials for supercapacitors. *J. Energy Storage* **2023**, *72*, 108544. [[CrossRef](#)]
59. Alnasrawi, F.A.; Mohammed, A.A.; Al-Musawi, T.J. Synthesis, characterization and adsorptive performance of CuMgAl-layered double hydroxides/montmorillonite nanocomposite for the removal of Zn(II) ions. *Environ. Nanotechnol. Monit. Manag.* **2023**, *19*, 100771. [[CrossRef](#)]
60. Xiong, C.; Cao, W.; Long, Q.; Chen, J.; Yu, Y.; Lian, X.; Huang, J.; Du, G.; Chen, N. Etching-induced ion exchange engineering of two-dimensional layered NiFeCo-based hydroxides for high energy charge storage. *Dalton Trans.* **2024**, *53*, 1295–1306. [[CrossRef](#)]
61. Al-Jamimi, H.A.; Bahadi, S.A.; BinMakhashen, G.M.; Onaizi, S.A. Optimal hybrid artificial intelligence models for predicting the adsorptive removal of dyes and phenols from aqueous solutions using an amine-functionalized graphene oxide/layered triple hydroxide nanocomposite. *J. Mol. Liq.* **2023**, *391*, 123374. [[CrossRef](#)]
62. Abdel-Hady, E.E.; Mohamed, H.F.M.; Hafez, S.H.M.; Fahmy, A.M.M.; Magdy, A.; Mohamed, A.S.; Ali, E.O.; Abdelhamed, H.R.; Mahmoud, O.M. Textural properties and adsorption behavior of Zn–Mg–Al layered double hydroxide upon crystal violet dye removal as a low cost, effective, and recyclable adsorbent. *Sci. Rep.* **2023**, *13*, 6435. [[CrossRef](#)]
63. Zaghouane-Boudiaf, H.; Boutahala, M.; Arab, L. Removal of methyl orange from aqueous solution by uncalcined and calcined MgNiAl layered double hydroxides (LDHs). *Chem. Eng. J.* **2012**, *187*, 142–149. [[CrossRef](#)]
64. Waheed, T.; Din, S.u.; Ming, L.; Ahmad, P.; Min, P.; Haq, S.; Khandaker, M.U.; Boukhris, I.; Faruque, M.R.I.; Rehman, F.U.; et al. Porous Hierarchical Ni/Mg/Al Layered Double Hydroxide for Adsorption of Methyl Orange from Aqueous Solution. *Nanomaterials* **2023**, *13*, 1943. [[CrossRef](#)] [[PubMed](#)]
65. Kim, M.; Kim, S.; Ahn, H.; Koh, Y.; Kim, K.; Lee, M.K.; Lee, J.W.; Kang, Y.T. Investigation on sacrificial hydrolysis reaction of octadecyltrimethoxysilane for moisture resistance enhancement of metal–organic framework. *Sep. Purif. Technol.* **2024**, *350*, 127957. [[CrossRef](#)]

66. Yuan, C.; Xiong, S.; Zhang, X.; Shen, L.; Zhang, F.; Gao, B.; Su, L. Template-free synthesis of ordered mesoporous NiO/poly(sodium-4-styrene sulfonate) functionalized carbon nanotubes composite for electrochemical capacitors. *Nano Res.* **2009**, *2*, 722–732. [CrossRef]
67. Wang, D.; Xu, R.; Wang, X.; Li, Y. NiO nanorings and their unexpected catalytic property for CO oxidation. *Nanotechnology* **2006**, *17*, 979. [CrossRef] [PubMed]
68. Zhang, J.T.; Liu, S.; Pan, G.L.; Li, G.R.; Gao, X.P. A 3D hierarchical porous α -Ni(OH)₂/graphite nanosheet composite as an electrode material for supercapacitors. *J. Mater. Chem. A* **2014**, *2*, 1524–1529. [CrossRef]
69. Winiarski, J.; Tylus, W.; Winiarska, K.; Szczygieł, I.; Szczygieł, B. XPS and FT-IR Characterization of Selected Synthetic Corrosion Products of Zinc Expected in Neutral Environment Containing Chloride Ions. *J. Spectrosc.* **2018**, *2018*, 2079278. [CrossRef]
70. Wang, M.; Jiang, L.; Kim, E.J.; Hahn, S.H. Electronic structure and optical properties of Zn(OH)₂: LDA + U calculations and intense yellow luminescence. *RSC Adv.* **2015**, *5*, 87496–87503. [CrossRef]
71. Ghaedi, M.; Khafri, H.Z.; Asfaram, A.; Goudarzi, A. Response surface methodology approach for optimization of adsorption of Janus Green B from aqueous solution onto ZnO/Zn(OH)₂-NP-AC: Kinetic and isotherm study. *Spectrochim. Acta Part A Mol. Biomol. Spectrosc.* **2016**, *152*, 233–240. [CrossRef]
72. Hobosyan, M.A.; Yolchinyan, S.A.; Martirosyan, K.S. A novel nano-energetic system based on bismuth hydroxide. *RSC Adv.* **2016**, *6*, 66564–66570. [CrossRef]
73. Liu, S.; Ren, G.; Gao, X.; Li, Z.; Wang, L.; Meng, X. A novel bismuth hydroxide (Bi(OH)₃) semiconductor with highly-efficient photocatalytic activity. *Chem. Commun.* **2022**, *58*, 8198–8201. [CrossRef] [PubMed]
74. Zhang, W.; Huang, X.; Tan, Y.; Gao, Y.; Wu, J.; Hu, J.; Stein, A.; Tang, B. A facile approach to prepare Bi(OH)₃ nanoflakes as high-performance pseudocapacitor materials. *New J. Chem.* **2015**, *39*, 5927–5930. [CrossRef]
75. Huang, H.; Wang, H.-L.; Jiang, W.-F. Solar-driven Bi₆O₅(OH)₃(NO₃)₅(H₂O)₃/Bi₂WO₆ heterojunction for efficient degradation of organic pollutants: Insights into adsorption mechanism, charge transfer and degradation pathway. *Sep. Purif. Technol.* **2024**, *349*, 127747. [CrossRef]
76. Zeng, X.; Cai, Z.; Zhang, C.; Wang, D.; Xu, J.; Wang, X. Novel NiFe-LDH@Ni-MOF/NF heterostructured electrocatalysts for efficient oxygen evolution. *Mater. Res. Lett.* **2022**, *10*, 88–96. [CrossRef]
77. Jian, W.; Jin, Z.; Yang, J.; Meng, G.; Liu, H.; Liu, H. Anticorrosion and antibiofouling performance of in-situ prepared layered double hydroxide coating modified by sodium pyrithione on aluminum alloy 7075. *J. Ind. Eng. Chem.* **2022**, *113*, 419–430. [CrossRef]
78. Manríquez, M.E.; Hernández-Cortez, J.G.; Wang, J.A.; Chen, L.F.; Zuñiga-Moreno, A.; Gómez, R. Synthesis of transition metal doped lamellar double hydroxides as base catalysts for acetone aldol condensation. *Appl. Clay Sci.* **2015**, *118*, 188–194. [CrossRef]
79. Xu, J.; Song, Y.; Tan, Q.; Jiang, L. Chloride absorption by nitrate, nitrite and aminobenzoate intercalated layered double hydroxides. *J. Mater. Sci.* **2017**, *52*, 5908–5916. [CrossRef]
80. Abo El-Reesh, G.Y.; Farghali, A.A.; Taha, M.; Mahmoud, R.K. Novel synthesis of Ni/Fe layered double hydroxides using urea and glycerol and their enhanced adsorption behavior for Cr(VI) removal. *Sci. Rep.* **2020**, *10*, 587. [CrossRef]
81. Li, J.; Zhang, S.; Chen, Y.; Liu, T.; Liu, C.; Zhang, X.; Yi, M.; Chu, Z.; Han, X. A novel three-dimensional hierarchical CuAl layered double hydroxide with excellent catalytic activity for degradation of methyl orange. *RSC Adv.* **2017**, *7*, 29051–29057. [CrossRef]
82. Spectroscopy of Carboxylic Acids and Nitriles. Available online: <https://chem.libretexts.org/@go/page/448775> (accessed on 8 November 2024).
83. Kudo, S.; Nakashima, S. Changes in IR band areas and band shifts during water adsorption to lecithin and ceramide. *Spectrochim. Acta Part A: Mol. Biomol. Spectrosc.* **2020**, *228*, 117779. [CrossRef]
84. Nait-Merzoug, A.; Guellati, O.; Djaber, S.; Habib, N.; Harat, A.; El-Haskouri, J.; Begin, D.; Guerioune, M. Ni/Zn Layered Double Hydroxide (LDH) Micro/Nanosystems and Their Azorubine Adsorption Performance. *Appl. Sci.* **2021**, *11*, 8899. [CrossRef]
85. Ouyang, Y.; Xu, Y.; Zhao, L.; Deng, M.; Yang, P.; Peng, G.; Ke, G. Preparation of ZnNiAl-LDHs microspheres and their adsorption behavior and mechanism on U(VI). *Sci. Rep.* **2021**, *11*, 21625. [CrossRef] [PubMed]
86. Rego, R.M.; Sriram, G.; Ajeya, K.V.; Jung, H.-Y.; Kurkuri, M.D.; Kigga, M. Cerium based UiO-66 MOF as a multipollutant adsorbent for universal water purification. *J. Hazard. Mater.* **2021**, *416*, 125941. [CrossRef]
87. Lade, H.; Kadam, A.; Paul, D.; Govindwar, S. A Low-Cost Wheat Bran Medium for Biodegradation of the Benzidine-Based Carcinogenic Dye Trypan Blue Using a Microbial Consortium. *Int. J. Environ. Res. Public Health* **2015**, *12*, 3480–3505. [CrossRef] [PubMed]
88. Malik, P.K. Dye removal from wastewater using activated carbon developed from sawdust: Adsorption equilibrium and kinetics. *J. Hazard. Mater.* **2004**, *113*, 81–88. [CrossRef]
89. Zubair, M.; Aziz, H.A.; Ahmad, M.A.; Ihsanullah, I.; Al-Harathi, M.A. Adsorption and reusability performance of M-Fe (M = Co, Cu, Zn and Ni) layered double hydroxides for the removal of hazardous Eriochrome Black T dye from different water streams. *J. Water Process Eng.* **2021**, *42*, 102060. [CrossRef]
90. Tabti, H.A.; Ammam, A.; Guezzen, B.; Boudinar, M.; Kadeche, A.; Ramdani, A.; Doumi, B.; Ech-Chergui, A.N.; Boudia, R.A.; Adjdir, M. Exploring the potential of Cu-LDHs composite for efficient Coomassie brilliant blue dye removal: Evaluating adsorption isotherms and antibacterial activity. *Res. Chem. Intermed.* **2024**, *50*, 2793–2825. [CrossRef]

91. Sardi, A.; Bounaceur, B.; Mokhtar, A.; Boukoussa, B.; Abbes, M.T.; Chaibi, W.; Nacer, A.; Khadidja, K.B.; Issam, I.; Iqbal, J.; et al. Kinetics and Thermodynamic Studies for Removal of Trypan Blue and Methylene Blue from Water Using Nano Clay Filled Composite of HTAB and PEG and its Antibacterial Activity. *J. Polym. Environ.* **2023**, *31*, 5065–5088. [[CrossRef](#)]
92. Karthikeyan, P.; Nikitha, M.; Pandi, K.; Meenakshi, S.; Park, C.M. Effective and selective removal of organic pollutants from aqueous solutions using 1D hydroxyapatite-decorated 2D reduced graphene oxide nanocomposite. *J. Mol. Liq.* **2021**, *331*, 115795. [[CrossRef](#)]
93. Nadaroglu, H.; Cicek, S.; Gungor, A.A. Removing Trypan blue dye using nano-Zn modified Luffa sponge. *Spectrochim. Acta Part A Mol. Biomol. Spectrosc.* **2017**, *172*, 2–8. [[CrossRef](#)]
94. Priyadarshini, B.; Patra, T.; Sahoo, T.R. An efficient and comparative adsorption of Congo red and Trypan blue dyes on MgO nanoparticles: Kinetics, thermodynamics and isotherm studies. *J. Magnes. Alloys* **2021**, *9*, 478–488. [[CrossRef](#)]
95. Sismanoglu, T.; Aroguz, A.Z. Adsorption kinetics of diazo-dye from aqueous solutions by using natural origin low-cost biosorbents. *Desalination Water Treat.* **2015**, *54*, 736–743. [[CrossRef](#)]
96. Wang, X.; Liu, Z.; Ye, X.; Hu, K.; Zhong, H.; Yu, J.; Jin, M.; Guo, Z. A facile one-step approach to functionalized graphene oxide-based hydrogels used as effective adsorbents toward anionic dyes. *Appl. Surf. Sci.* **2014**, *308*, 82–90. [[CrossRef](#)]
97. Prabhu, S.M.; Khan, A.; Hasmath Farzana, M.; Hwang, G.C.; Lee, W.; Lee, G. Synthesis and characterization of graphene oxide-doped nano-hydroxyapatite and its adsorption performance of toxic diazo dyes from aqueous solution. *J. Mol. Liq.* **2018**, *269*, 746–754. [[CrossRef](#)]

Disclaimer/Publisher's Note: The statements, opinions and data contained in all publications are solely those of the individual author(s) and contributor(s) and not of MDPI and/or the editor(s). MDPI and/or the editor(s) disclaim responsibility for any injury to people or property resulting from any ideas, methods, instructions or products referred to in the content.